NASA CONTRACTOR REPORT

NASA CR-130

NASA CR-130

RESEARCH ON NON-MAGNETIC POWER SUPPLIES

by John L. Artley and James E. Hall, Jr.

Prepared under Grant No. NsG-251-62 *by*
DUKE UNIVERSITY
Durham, N. C.
for

NATIONAL AERONAUTICS AND SPACE ADMINISTRATION • WASHINGTON, D. C. • NOVEMBER 1964

RESEARCH ON NON-MAGNETIC POWER SUPPLIES

By John L. Artley and James E. Hall, Jr.

Prepared under Grant No. NsG-251-62 by
DUKE UNIVERSITY
Durham, North Carolina

for

NATIONAL AERONAUTICS AND SPACE ADMINISTRATION

For sale by the Office of Technical Services, Department of Commerce,
Washington, D.C. 20230 -- Price $1.75

FORWORD

This is a report of a study of components which may be used in a non-magnetic converter.* A new oscillator design with an 80 percent efficiency is described. The analysis and testing of a model for a distributed winding, toroidal, air-core transformer indicates a reasonable check in calculated and experimental results over a frequency range from 10 to 100 kilocycles. The stray magnetic field of the transformer near resonance is approximately ten times the stray magnetic field at off-resonance frequencies. Results also show that the characteristics of the transformer are markedly sensitive to load.

A number of appendices are included with the report giving the detailed development of the analytical model used to predict the characteristics of the toroidal, air-core transformer. Results from the analytical model were obtained from computations using the facilities of the Duke University Digital Computer Laboratory.

*Non-magnetic means no ferromagnetic materials are used and the converter configurations are designed to minimize magnetic interference external to the converter.

TABLE OF CONTENTS

LIST OF APPENDICES

LIST OF TABLES*

*Tables 1 through 10 compare analytical values (calculated) and experimental values obtained by measurement. Tables 1 through 5 correspond to a load impedance of 1000 ohms and Tables 6 through 10 correspond to a load impedance of 30,400 ohms.

LIST OF FIGURES

RESEARCH ON NON-MAGNETIC POWER SUPPLIES

By John L. Artley and James E. Hall, Jr.

SUMMARY

10951

This is a report describing work accomplished in the study of components for use in a non-magnetic converter.* A new oscillator utilizing 4 transistors in a bridge arrangement is reported to have a maximum efficiency near 80 percent when operating over a range of frequencies from 7 to 30 kilocycles. The analysis and experimental testing of toroidal, distributed winding, air core transformers exhibits a reasonably good correlation over a range of frequencies from 10 to 100 kilocycles.

An equivalent circuit is developed and parameters of the circuit are calculated from the size and shape of materials in the toroidal configuration. The equations and calculations involving circuit parameters and circuit response are of a complexity which requires the use of a digital computer to yield analytical results in a reasonable time.

Tables and graphs present analytical and experimental results describing input impedance, efficiency, transfer function, resonant frequencies, and external magnetic fields. Results indicate the transformers are quite sensitive to load. The stray magnetic field of the transformer operating near resonance is approximately 10 times the stray magnetic field at off-resonance frequencies.

AUTHOR

*Non-magnetic means no ferromagnetic materials are used and the converter configurations are designed to minimize magnetic interference external to the converter.

INTRODUCTION

The design of D. C. to D. C. converters with negligible magnetic interference characteristics has become necessary in view of current need for satellite power systems that will permit the undistorted measurement of the very small magnetic fields existing in outer space.

Conventional satellite power systems utilize ferromagnetic components to achieve voltage conversion and inversion. These components impair the accuracy of magnetic field measurements in two ways:

(1) The ambient field is distorted by the presence of the relatively high permeability of the ferromagnetic material.

(2) Ferromagnetic materials exhibit a residual magnetic field that may be greater than or equal, in order of magnitude, to the ambient field.

The possibility of shielding is limited due to the essentially static nature of both the ambient and residual fields, and this has forced the consideration of other possible means of achieving voltage transformations, not using ferromagnetic materials.

At present, two general methods for achieving voltage transformation are being explored, the ceramic transformer and the inductively coupled, air-core transformer operating in the radio frequency range. A specific air-core transformer configuration is considered in this report.

PRELIMINARY CONSIDERATIONS

A first Semi-Annual Status Report, submitted to the National Aeronautics and Space Administration on October 3, 1962, presented a brief analysis of a new oscillator design capable of operating at efficiences near 80 percent and having a square wave output, the frequency of which was a logarithmic function of the base drive of the transistors (see appendix E). This oscillator was developed to serve as the driver stage for a non-magnetic converter. Due to the anticipated low efficiency of the transformer stage of the converter, considerable effort was made to maximize the efficiency of this design as a first step in obtaining maximum efficiency in the overall converter.

It is generally accepted that toroidal windings produce magnetic fields which are confined primarily within the volume

of the toroid. Therefore, in order to minimize the value of the induced magnetic field external to the windings, and to reduce or eliminate the problem of shielding, the toroid was chosen for the basic transformer configuration.

With the basic geometry fixed, the choice of winding arrangement was dictated by the following considerations.

(1) The placement of the windings must be such as not to destroy the field confining properties of the basic geometry.

(2) The design must be amenable to analytical study and should not require unreasonably close tolerances for successful fabrication.

(3) In order to obtain the highest possible efficiency, the coupling constant must be maximized insofar as is consistent with the requirements of (1) and (2) above.

Three types of windings were considered initially.

(1) A primary winding consisting of a copper sheet which encloses the toroid and the secondary (uniformly distributed) winding, and having a small gap along the inner circumference of the toroid. The primary input leads come in as a twisted pair to the center of toroid and from there branch out to a number of points along the gap so as to insure as nearly uniform a current distribution as possible. The secondary winding terminals are brought out through the gap. This copper sheet acts as a single turn, perfectly distributed primary winding.

(2) Segmented bank windings, spaced symmetrically around the toroid.

(3) Uniformly distributed, multi-layer windings.

SINGLE TURN PRIMARY

Initially, the single turn primary was regarded with considerable enthusiasm. This type of primary places a "current sheet" around the enclosed secondary windings. Therefore, the external magnetic field of this device is a direct function of the length of the gap in the primary winding, which can be made quite small. Hence, a device of this type would exhibit a very low leakage field. Such a device was built and tested. The data showed very low values for the magnitude of the primary

to secondary voltage transfer function and the transformer efficiency. An analytical model was postulated for this device and the analytical results showed close agreement with the experimental data. Predictions taken from the model indicate that the inherently low value of primary inductance limits the maximum obtainable efficiency of this device to approximately ten percent and the radial dimensions of the toroid must be of the order of twenty fold to achieve even this modest value. These facts clearly eliminate the single turn primary from consideration as a practical device.

SEGMENTED BANK WINDING

The segmented bank windings were rejected in favor of uniformly distributed windings due to the fabrication and analysis criterion mentioned previously. The uniformly distributed windings are easier to reproduce and their circuit equivalent is more easily obtained.

DISTRIBUTED TOROIDAL WINDINGS

As stated previously, the toroidal shape of the distributed windings acts to confine the induced field of the transformer. The use of distinct turns, as opposed to the single turn arrangement, introduces additional considerations due to the manner in which the current flows around the surface of the toroid. Taking an axis perpendicular to the plane of the toroid and passing through the center of the toroid, form a cylindrical coordinate system about this axis. It is clear that the current density in the windings will have components in all three coordinate directions. The field created by the axial and radial components of current density is confined to the volume of the toroid but the theta directed component creates a field that is not confined to within the toroid. Methods of estimating the order of magnitude of this field have been developed and are presented in some detail in Appendix D.

ANALYSIS

Figure 1 shows the equivalent circuit that has been derived for the uniformly distributed, mutually coupled, toroidal windings. This is a lumped parameter approximation to the behavior of the actual distributed system, and the methods whereby it is derived are presented in detail in Appendix A.

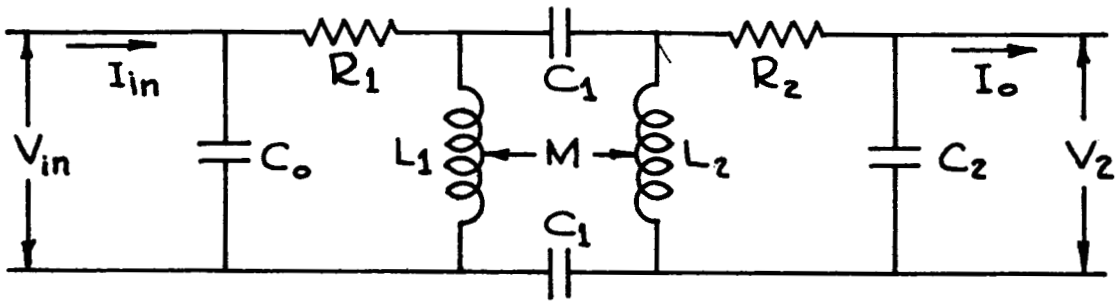

Figure 1: The Equivalent Circuit for the Distributed Winding Transformer.

The following frequency dependent characteristics of the distributed winding model are obtained by Laplace methods in Appendix B.

(a) Magnitude of the input impedance, ($|Z_{in}|$).

(b) Phase angle of the input impedance, ($\Phi(Z_{in})$).

(c) Magnitude of the voltage transfer function, ($|G_v|$).

(d) Phase angle of the transfer function, ($\Phi(G_v)$).

(e) Efficiency of the power transfer between the primary and secondary parts, (E).

Two more important characteristics of the model are obtained in appendices B and D. In Appendix B, the resonant frequencies of the device are found as the solutions of an eighth order polynomial. In Appendix D, a static field model is postulated and predictions are made for the axially directed component of the magnetic field.

In order to test the validity of the analysis, two transformer models (T1 and T2) were designed, built, and tested and the experimental results were compared with the analytical results. The physical nature of the designs T1 and T2 are described in Appendix F.

Both T1 and T2 were tested using two very different values of load resistance. For the first test, Z_L was set equal to 1000 ohms, and for the second case, Z_L was fixed at 30,400 ohms. The analytical and experimental results are compared in tables 1 through 11.

Case 1: Z_L = 1000 ohms (Tables 1 through 5):

TABLE 1

(a) Magnitude of Input Impedance, Z_{in} (ohms)

T1		T2		
ANAL.	EXP.	ANAL.	EXP.	frequency (kcps)
79.1	78.6	28.0	28.8	10
152	151	44.0	44.0	20
219	218	57.8	57.2	30
275	273	71.8	72.1	40
328	327	86.3	87.3	50
374	373	101.3	102	60
398	396	116.6	118	70
422	420	132.4	134	80
435	433	148.4	149	90
433	431	164.8	164	100

TABLE 2

(b) Phase Angle of Input Impedance, $\Phi(Z_{in})$ (radians)

T1		T2		
ANAL.	EXP.	ANAL.	EXP.	frequency (kcps)
1.27	1.26	1.045	1.02	10
1.20	1.18	1.055	1.03	20
1.08	1.06	1.13	1.07	30
0.944	0.872	1.187	1.15	40
0.784	0.746	1.225	1.18	50
0.708	0.569	1.250	1.21	60
0.382	0.494	1.258	1.22	70
0.192	0.455	1.260	1.24	80
0.172	0.429	1.265	1.25	90
0.141	0.428	1.270	1.23	100

TABLE 3

(c) Magnitude of the Voltage Transfer Function, G_v

T1 ANAL.	T1 EXP.	T2 ANAL.	T2 EXP.	frequency (kcps)
1.26	1.24	2.94	3.06	10
1.24	1.23	2.55	2.63	20
1.22	1.21	2.09	2.20	30
1.21	1.20	1.74	1.89	40
1.21	1.19	1.47	1.60	50
1.14	1.14	1.26	1.36	60
1.13	1.13	1.10	1.18	70
1.13	1.12	0.98	1.01	80
1.11	1.12	0.87	0.89	90
1.10	1.10	0.78	0.80	100

TABLE 4

(d) Efficiency (%)

T1 ANAL.	T1 EXP.	T2 ANAL.	T2 EXP.	frequency (kcps)
41.5	40.8	48.1	46.3	10
64.1	63.0	58.1	56.7	20
68.3	68.0	59.4	57.4	30
68.3	68.0	58.2	57.2	40
66.1	65.6	55.0	53.1	50
64.6	63.4	51.4	49.3	60
55.0	52.7	45.5	42.9	70
54.8	51.6	41.2	37.3	80
54.2	51.0	37.4	33.5	90
53.9	49.0	34.7	30.4	100

TABLE 5

(e) Resonant Frequencies

T1 ANAL.	T1 EXP.	T2 ANAL.	T2 EXP.
917 KC	896 KC = f_1	623 KC	609 KC = f_1

Case 2: Z_L = 30,400 ohms: (Tables 6 through 10):

TABLE 6

(a) Magnitude of the Input Impedance, Z_{in} (ohms)

T1		T2		frequency
ANAL.	EXP.	ANAL.	EXP.	(kcps)
77.4	76.2	30.7	30.4	10
157	155	60.6	60.0	20
245	244	91.5	89.3	30
344	340	123.5	121.1	40
444	442	157.1	155.4	50
569	566	192.9	191.7	60
704	698	232	230	70
780	774	274	275	80
929	922	321	320	90
1061	1052	375	372	100

TABLE 7

(b) Phase Angle of the Input Impedance, $\phi(Z_{in})$ (radians)

T1		T2		frequency
ANAL.	EXP.	ANAL.	EXP.	(kcps)
1.30	1.30	1.00	1.01	10
1.43	1.39	1.03	1.04	20
1.40	1.38	1.05	1.05	30
1.36	1.35	1.06	1.06	40
1.33	1.30	1.07	1.06	50
1.28	1.24	1.11	1.09	60
1.22	1.14	1.13	1.11	70
1.19	1.10	1.18	1.10	80
1.13	1.05	1.12	1.08	90
1.10	1.00	1.10	1.06	100

TABLE 8

(c) Magnitude of the Voltage Transfer Function, G_v

T1 ANAL.	T1 EXP.	T2 ANAL.	T2 EXP.	frequency (kcps)
1.29	1.30	3.51	3.55	10
1.33	1.34	3.61	3.64	20
1.29	1.30	3.66	3.68	30
1.27	1.27	3.72	3.74	40
1.25	1.26	3.80	3.81	50
1.24	1.25	3.90	3.92	60
1.23	1.23	4.02	4.05	70
1.21	1.22	4.17	4.20	80
1.20	1.20	4.36	4.37	90
1.18	1.19	4.60	4.63	100

TABLE 9

(d) Efficiency (%)

T1 ANAL.	T1 EXP.	T2 ANAL.	T2 EXP.	frequency (kcps)
1.63	1.5	5.41	5.28	10
5.90	5.3	15.2	15.05	20
7.62	7.3	23.9	23.7	30
8.53	8.4	28.2	27.7	40
9.41	9.3	30.5	29.4	50
9.90	9.8	32.8	30.8	60
10.21	10.1	34.0	31.1	70
10.30	10.2	34.2	31.9	80
10.35	10.3	34.8	32.3	90
10.9	10.7	35.6	33.5	100

TABLE 10

(e) Resonant Frequencies

T1

ANAL.	EXP.
f_1 = 194 kilocycles	f_1 = 186.0 kilocycles
f_2 = 590 "	f_2 = 584.0 "
f_3 = 983 "	f_3 = 904 "

T2

ANAL.	EXP.
f_1 = 162 kilocycles	f_1 = 153.0 kilocycles
f_2 = 609 "	f_2 = 597.0 "

The analytical determination of the magnetic leakage field at a distance of 0.5 meter with a current of 1.0 ampere in the secondary winding was made for the model T2, and yielded the following.

TABLE 11

Stray Magnetic Field

H_z (gammas)	θ (degrees)
8.39	0.0
8.39	5.0
8.40	10.0
8.40	15.0
8.41	20.0
8.41	25.0
8.42	30.0
8.43	35.0
8.44	40.0
8.46	45.0
8.47	50.0
8.48	55.0
8.49	60.0
8.50	65.0
8.51	70.0
8.51	75.0
8.52	80.0
8.52	85.0
8.52	90.0

Note: 1 gamma = 10^{-5} gauss.

Where Θ is the azimuth angle (spherical coordinates)

An order of magnitude check was made on the magnetic leakage field calculations by using a small pick-up coil combined with a sensitive vacuum tube voltmeter. The leakage field was the same order of magnitude as calculated values at off resonance frequencies but near resonance the leakage field would increase ten fold.

Figures 2 through 5 provide a comparison of test and analytical results for the transformer T1.

DISCUSSION OF RESULTS

Comparison of the analytical predictions taken from the model and the experimental data shows varying degrees of accuracy. The magnitude of the input impedance exhibits excellent agreement over the entire range of 10 to 100 kilocycles, as does the magnitude of the transfer function. The calculated efficiencies are in reasonably good agreement over the lower portion of this frequency range, however, some divergence is noted near the 100 kilocycle frequency point. It is clear that the primary reason for the increasing error is in the predicted versus the actual phase angle of the input impedance, since the efficiency expression is divided by the cosine of this angle. The increasing error in the calculation of the phase angle of Z_{in} may be traced directly to the assumptions made to obtain the equivalent network of Figure 1. As discussed in Appendix A, it is necessary to approximate the behavior of a multiple loop distributed system by a single loop, lumped parameter equivalent. In the low R F band, the approximation is quite good and it is also good for extremely high R F, however, in the middle radio frequency range, the behavior of the multiple loop system is much more poorly approximated by the lumped system due to the fact that the many loop system has the possibility of producing a variety of resonance effects that cannot be achieved by the single loop equivalent. A multiple loop model of the distributed windings can be conceptualized but the computational labor involved in its solution increases very rapidly with increasing numbers of loops and it is doubtful if the obtainable increase in accuracy will justify the additional labor.

In its present form, the model exhibits sufficient accuracy to be useful as an analytical tool. The overall behavior of a given design can be estimated within ten percent from 1 to 100 kc. by this model and the effect of a changing load can readily be observed.

FIGURE 2. Magnitude of Input Impedance vs. Frequency, T_1

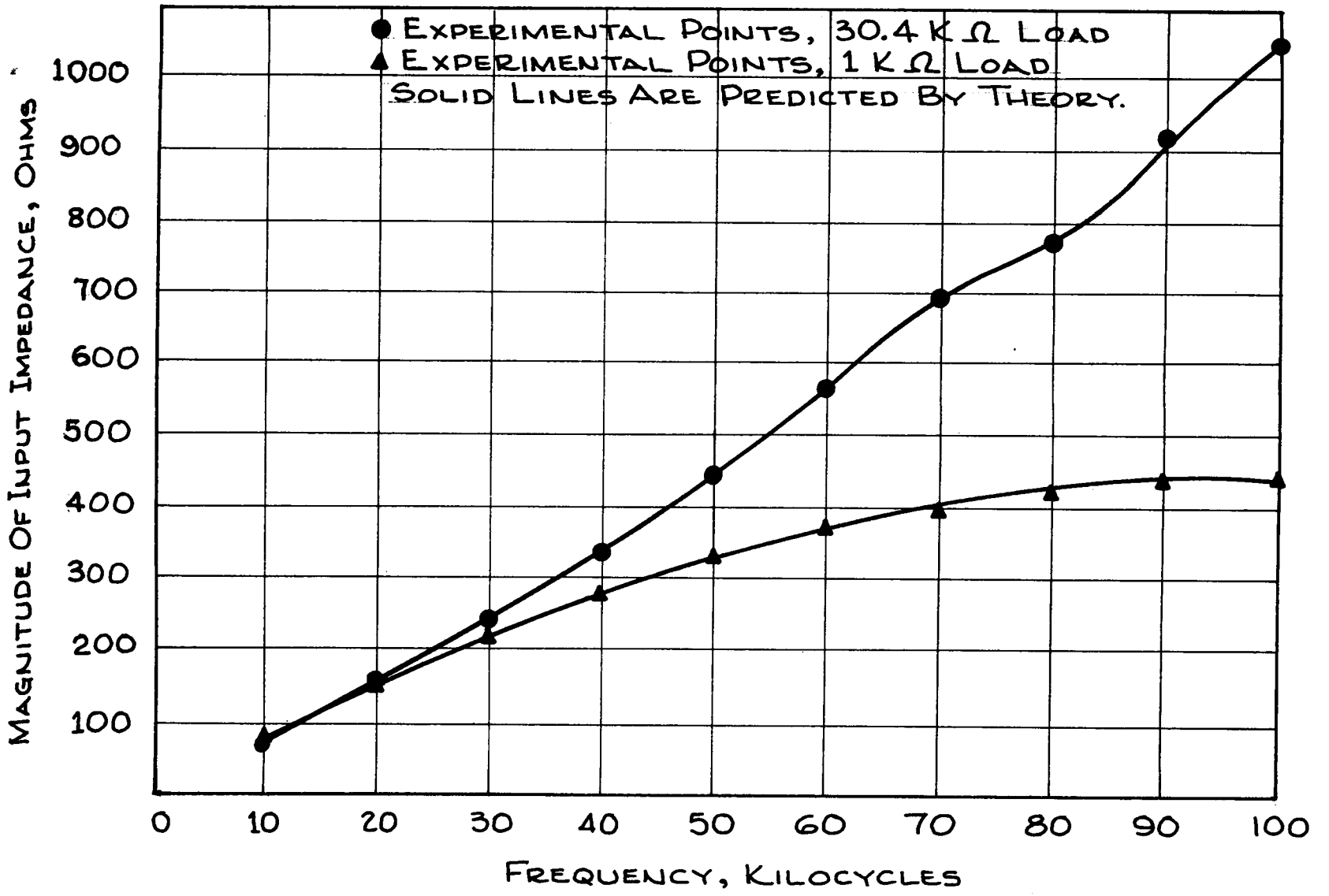

FIGURE 3. Phase Angle of Input Impedance vs. Frequency, T_1

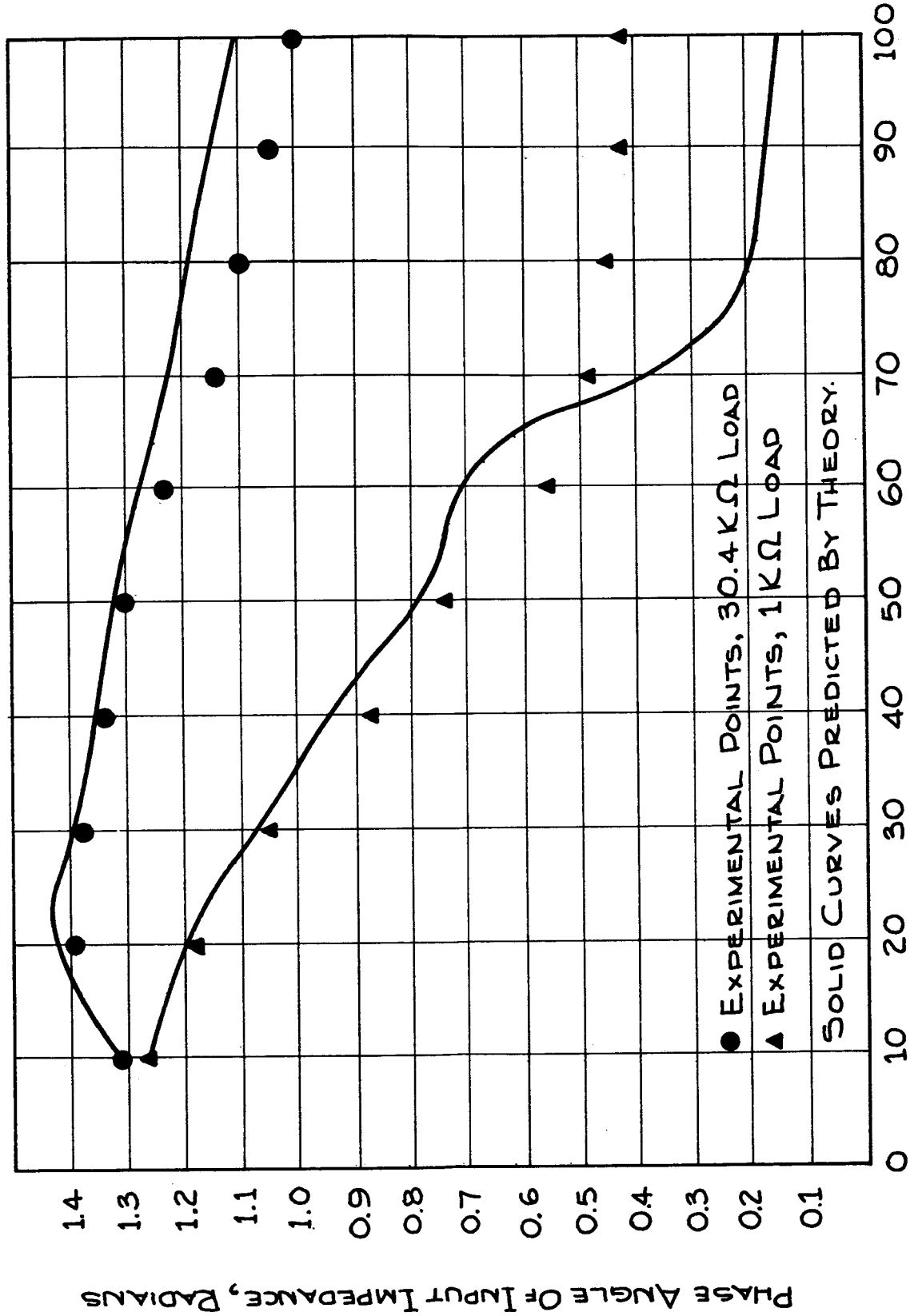

FIGURE 4. Magnitude of Transfer Function vs. Frequency, T_1

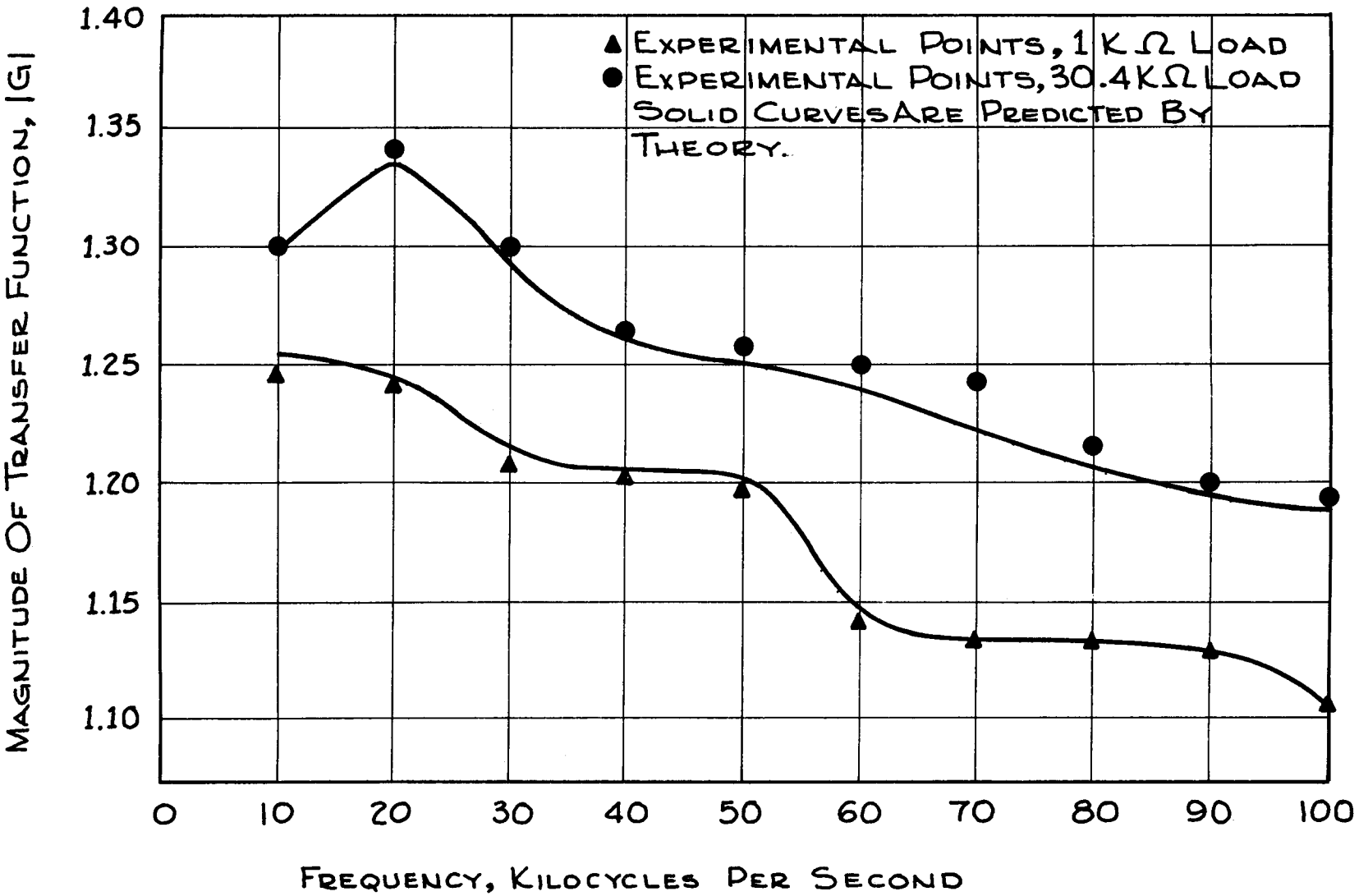

FIGURE 5. Efficiency vs. Frequency, T_1

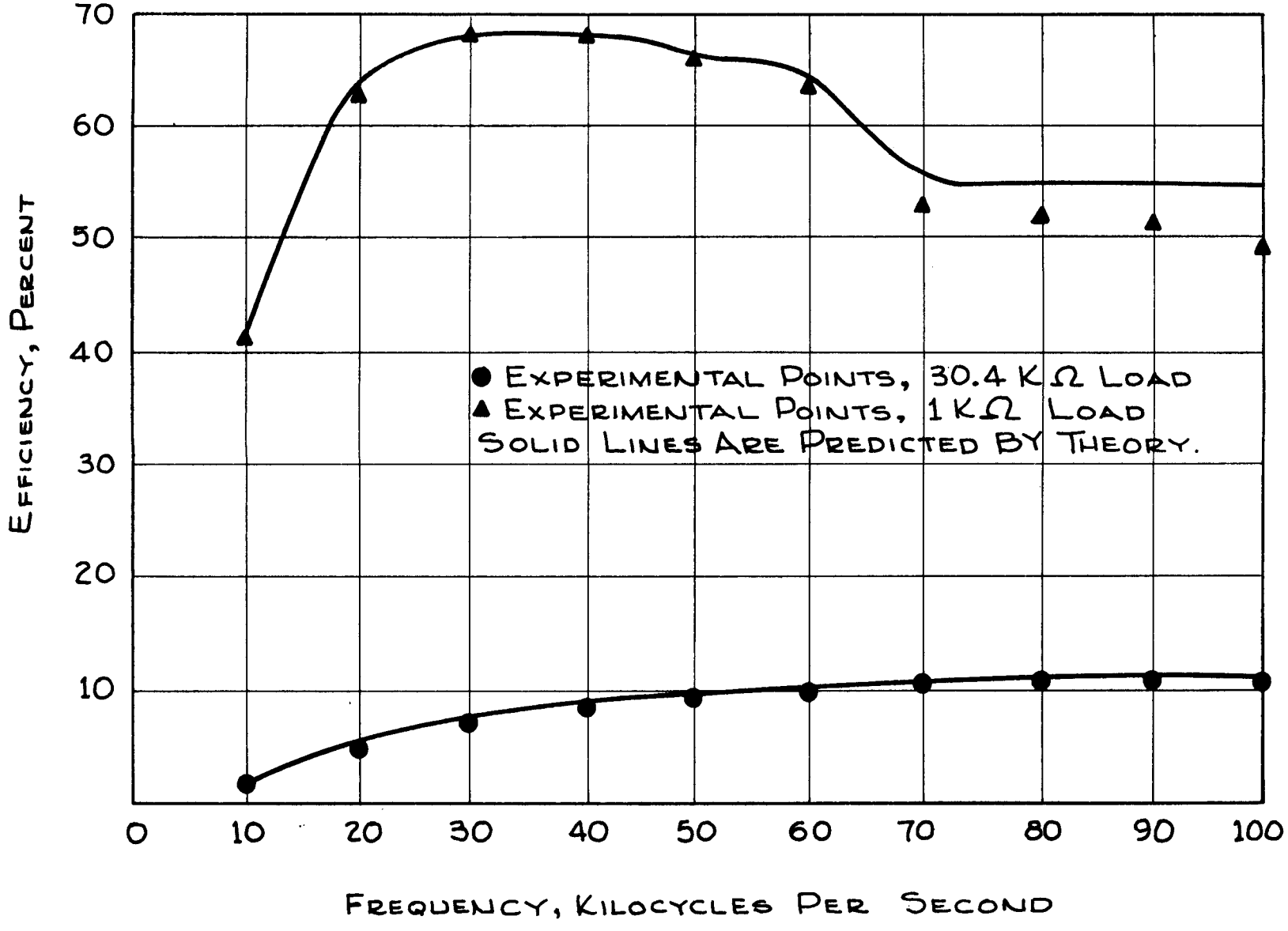

The resonant frequency polynomial given in Appendix B, is of interest due to the fact that it imposes an upper limit on the number of resonant frequencies a design may exhibit, namely, only four resonances are allowed. Again, looking at the multiple loop system, such a limitation seems inconsistent with the facts but all of the transformers examined in the course of this work have shown four or less resonances over the range 1000 cycles to ten megacycles. Furthermore, it appears that by changing the magnitude of the load resistance, some of these resonances may be eliminated.

COMMENTS

From the results of this work, several comments can be made concerning the use of the air-core transformer in converter systems. The decreasing efficiency for increasing values of load resistance indicates that the distributed winding transformer exhibits a rather low output impedance. Therefore, an impedance match and optimum efficiency can be achieved only by serving relatively low impedance loads. Thus far, the analysis does not allow for reactive loading, but it will be seen in Appendix B that only a minor change in the analysis will be necessary to account for reactive loads.

The shape of the plot of the magnitide of the voltage transfer function versus frequency raises some interesting possibilities for regulation when combined with the load-frequency characteristics of the driver oscillator discussed in Appendix E. The frequency of the driver increases with increasing load, therefore, if the operating point of the transformer is positioned on the rising portion of the G_V vs f curve, the drop in output terminal voltage due to an increase in load current would tend to be offset by an increase in the magnitude of the transfer function. As yet, no practical test of this hypothesis has been made but the possibility of achieving worthwhile voltage regulation seems to exist.

In general, the analytical model presented in this report requires a cut and try procedure to design converter components. A desirable result would be to invert the entire analysis process, thus achieving a synthesis method, wherein specifications could be imposed and a physical geometry determined. A first step has been taken in this direction in Appendix C, where all the partial derivatives of the network functions with respect to the network parameters have been computed as a function of frequency. By having some knowledge of the manner in which a change in one of the circuit

parameters affects the network functions, a designer can then examine the relationship of the parameter in question to the transformer geometry and adjust the geometry as best meets his needs.

CONCLUSIONS

An analytical model describing a distributed winding, air-core transformer has been developed and tested over a range of frequencies from 10 to 100 kilocycles. Experimental results check within 10 percent for input impedance, transfer function and efficiency. A resistive load has been used to indicate that the characteristics of the transformer are sensitive to load. Calculations and measurements of efficiency and stray magnetic fields indicate that it is undesirable to operate the transformer near resonance if high efficiencies and low leakage fields are desired. Appendix E describes an oscillator design having efficiencies of approximately 80 percent. This oscillator, used in conjunction with the transformer described in this report, offers the possibility of achieving self-regulation by combining the frequency dependent characteristics of the two devices.

REFERENCES

1. S. Ramo and J. R. Whinnery, Fields and Waves in Modern Radio, John Wiley and Sons, Inc. 2nd ed., New York, 1953.

2. P. M. Moon and D. E. Spencer, Field Theory for Engineers, D. Van Nostrand and Company, Inc., Princeton, New Jersey, 1961.

Appendix A

CALCULATION OF THE PARAMETERS OF THE EQUIVALENT CIRCUIT

The conceptual approach used to devise a circuit equivalent for the distributed winding model is based on the model proposed for the much simpler single turn primary design. The circuit shown in Figure A-1 was found to represent the primary of the single turn design with good accuracy. There is sufficient physical similarity between the two models to justify an attempt to fit this equivalent circuit to the behavior of the distributed winding configuration. This result was achieved in the following way.

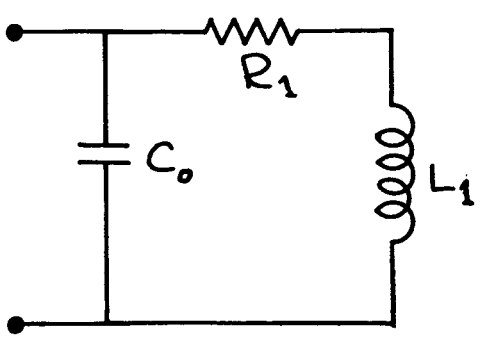

Figure A-1

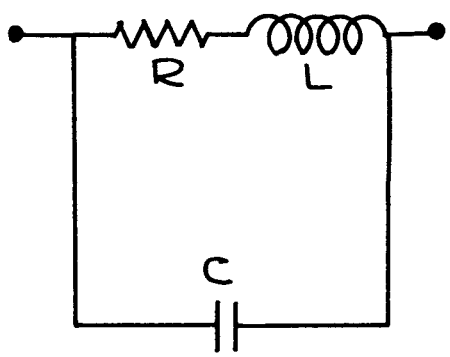

Figure A-2a

Figure A-2a gives the proposed equivalent circuit for a single turn of a distributed winding. There is a resistance per turn and an inductance per turn which appear in series. These elements are shunted by a turn to turn capacitance.

We begin the development of the model by considering the combination of these single turn equivalents to form a single layer of turns as shown in Figure A-2b. The mutual inductance that would appear between turns is symmetrical and each turn will have the same contribution to the mutual flux, therefore, for convenience, the effect of the mutual inductance is lumped with the self inductance and represented by L*. The values R and C are the same as for the single turn equivalent.

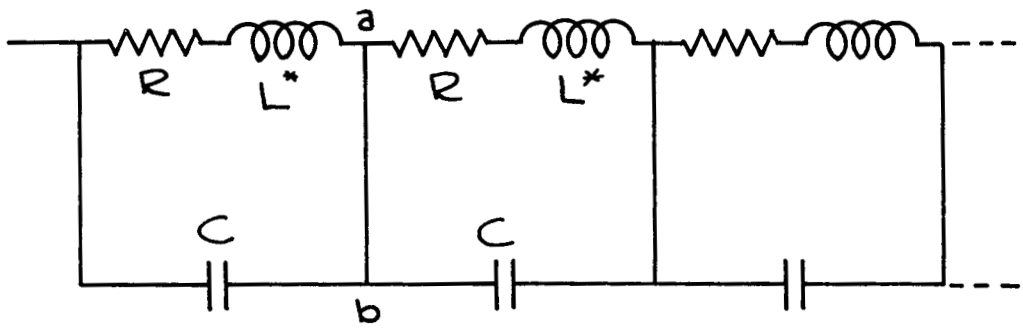

Figure A-2b

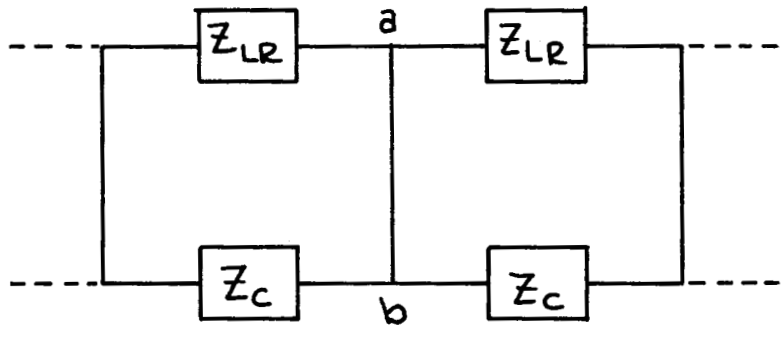

Figure A-2c

A close examination of Figure A-2b shows that each two successive segments form a "bridge" around the connections a,b. The net effect may be represented as shown in Figure A-2c. Z_{LR} is the series impedance of the inductor-resistor combination and Z_C is the impedance of the shunt capacitor. Clearly, the cross product of the arm impedances is equal and no current will flow in the line a,b hence, the a,b connection may be removed with no effect on the circuit performance, yielding the equivalent circuit shown in Figure A-2d which immediately reduces to the circuit shown in Figure A-2e with the following definitions obtaining.

$$L_s = NL^* \qquad \text{(A-1a)}$$

$$R_s = NR \qquad \text{(A-1b)}$$

$$C_s = C/N \qquad \text{(A-1c)}$$

where N is the number of turns in the layer.

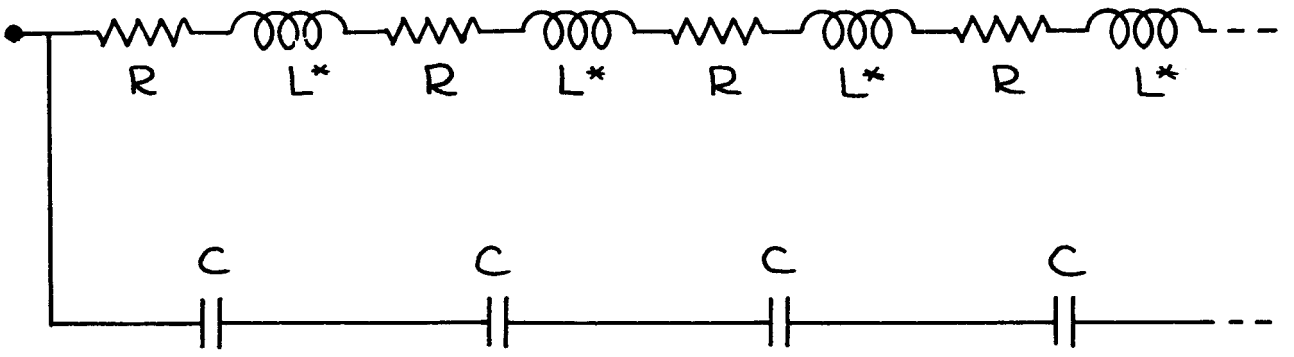

Figure A-2d

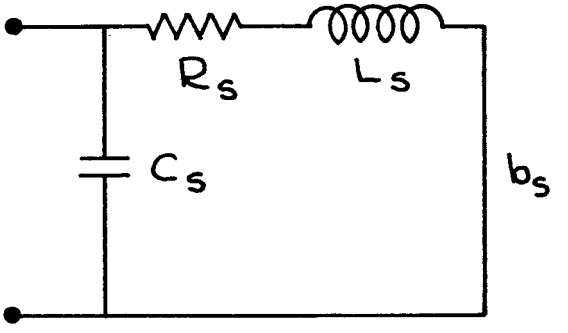

Figure A-2e

The next step in the development is to consider the case for many layers of turns. The circuit equivalent for this case is shown in Figure A-3a. C_{Lj} is the layer to layer capacitance and L_{Sj}* again represents the combined self and mutual inductance and R_{Sj} is as defined previously with j denoting the jth layer in all cases. Since the capacitances C_{Sj} and C_{Lj} are in parallel, they may be immediately combined to C_{Lj}* and the equivalent circuit reduced to that shown in Figure A-3b

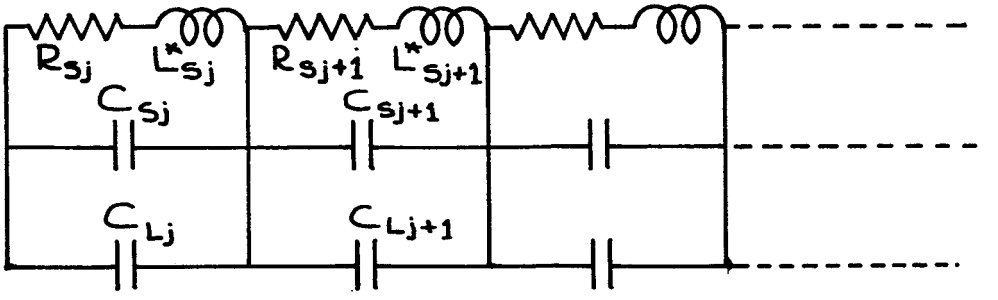

Figure A-3a

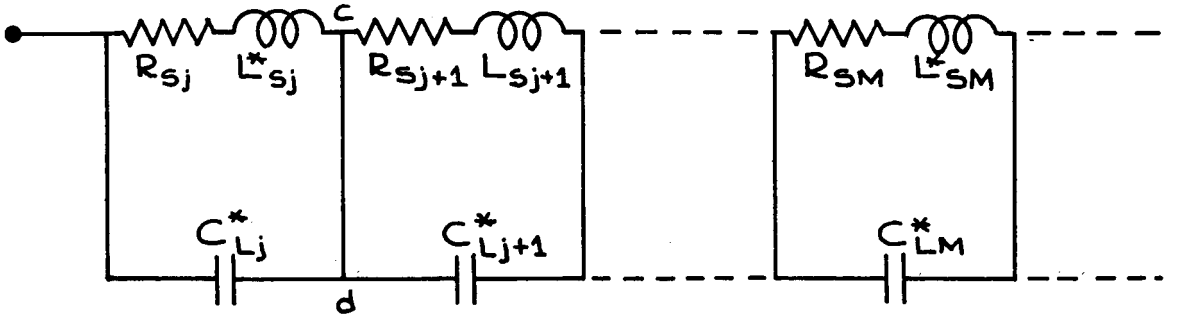

Figure A-3b

The situation is now similar to the case of a single layer of turns in that a bridge is now formed around each of the connections c,d. However, an approximation must now be made in order to remove the connections c,d. Although, the elements in the jth equivalent differ by a few percent from those in the (j + 1st) equivalent, to a first order approximation, the cross product of the impedances may be assumed to be equal and the connections c,d removed. This will reduce the circuit to the equivalent shown in Figure A-3c. Both the primary and secondary windings may be represented by a circuit of the type shown in Figure A-3c, therefore, the complete equivalent circuit is given by Figure A-3d, where C_1 in the interwinding capacitance and M is the coefficient of mutual conductance between the windings.

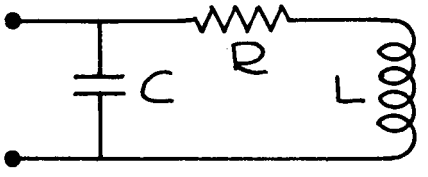

Figure A-3c

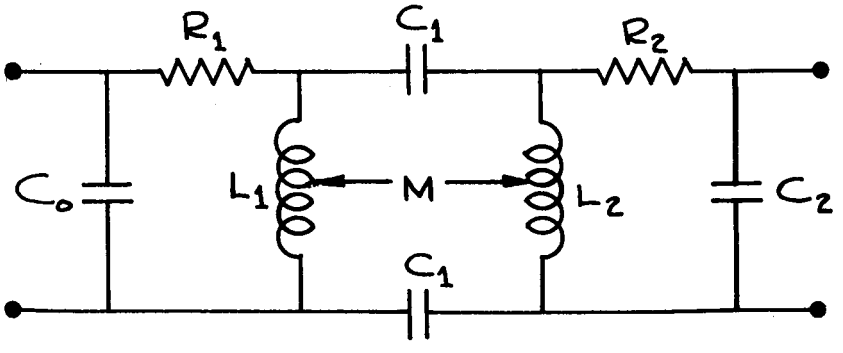

Figure A-3d

Calculation of the Parameters in the Equivalent Circuit.

a. Primary resistance

Examination of Figure A-3c shows that the equivalene resistance of the primary winding is the resistance of an equivalent length of primary conductor. To determine this value, we use the standard resistance formula:

$$R = \frac{\rho \ell}{A} \qquad \text{(A-2)}$$

where

R = resistance in units of ohms.

ℓ = length of conductor in units of meters.

A = cross-sectional area of conductor in units of meters.^{2}

ρ = resistivity of material in ohm-meters.

To aid in the development, we make the following definitions.

r = distance from the center of the torous to the center of the cross-section.

a = radius of the cross-section.

N_k = Number of <u>turns</u> in the kth layer.

n_p = Number of primary <u>layers</u>.

s as subscript refers to "secondary."

p as subscript refers to "primary."

$d\omega_p, d\omega_s$ = diameter of primary and secondary conductors, including insulation.

δ_p = thickness of insulation on primary conductor.

δ_s = thickness of insulation on secondary conductor.

σ = thickness of interlayer insulation.

A_p, A_s = cross sectional area of primary and secondary conductors without insulation in meters squared.

A^*_p, A^*_s = cross sectional area of primary and secondary conductors <u>including</u> insulation in circular mils.

a_j = cross sectional radius to the j^{th} layer of turns.

δ^*_p, δ^*_s = insulation thickness in mils.

The length of the primary conductor may be considered as the sum of the lengths of each layer of primary turns and the length in any one layer is equal to the number of turns multiplied by the length of one turn. The total length of a single turn in the k^{th} layer is given by

$$\ell_t = 2\pi \quad (a_k + d\omega_p/2) \tag{A-3}$$

where

$$a_k = a + k\,(d\omega_p + \sigma) - d\omega_p \tag{A-4}$$

Therefore,

$$\ell_t = 2\pi\,(a + k\,(d\omega_p + \sigma) - d\omega_p/2) \tag{A-5}$$

$$= 2\pi\,(a + d\omega_p\,(k - 1/2) + k\sigma) \tag{A-6}$$

Hence, the length of the k^{th} layer of conductor is given by:

$$\ell_k = N_K(2\pi)\,(a + d\omega_p(k - 1/2) + k\,\sigma) \tag{A-7}$$

Therefore, the total length of primary conductor is expressed by:

$$\ell_p = \sum_{k=1}^{n_p} \ell_k = 2\pi \sum_{k=1}^{n_p} N_k\,(a + d\omega_p\,(k - 1/2) + k\sigma) \tag{A-8}$$

where n_p is the total number of primary layers. The area of the primary conductor is expressed as:

$$A_p = (A^{*\,1/2}_p - 2\delta^*_p)^2\,K \tag{A-9}$$

where

$K = (2.54)^2\ (.25)(\pi)\ (10^{-10})$ (conversion factor from circular mils to sq, meters) (A-10)

Combining these results yields the following formula

$$R_1 = \frac{2\pi \sum_{k=1}^{n_p} N_k(a + d\omega_p\,(k - 1/2) + k\sigma)}{[(A^*_p)^{1/2} - 2\delta^*_p]^2\,K}\,\rho \tag{A-11}$$

Secondary Resistance R_2:

The calculation of R_2 proceeds in exactly the same manner except provision must be made for the additional length of conductor due to the presence of the primary winding. The expression for the length per turn of the ith layer of secondary turns is:

$$\ell_{ts} = 2\pi(a_i) \qquad \text{(A-12)}$$

where

$$a_i = a + n_p(d\omega_p + \sigma) + d\omega_s\ (i - 1/2) + i\sigma \qquad \text{(A-13)}$$

Therefore,

$$\ell_{ts} = 2\pi[a + n_p\ (d\omega_p + \sigma) + d\omega_s\ (i - 1/2) + i\sigma\ ] \qquad \text{(A-14)}$$

and the total length of conductor in the i^{th} layer is:

$$\ell_i = 2\pi N_i\ [a + n_p\ (d\omega_p + \sigma) + d\omega_s\ (i - 1/2) + i\sigma\ ].$$

The area is given by:

$$A_s = [(A^*_s)^{1/2} - 2\delta^*_s]^2\ .\ K \qquad \text{(A-15)}$$

Therefore,

$$R_2 = \frac{2\pi \sum_{i=1}^{n_s} N_i[a + n_p(d\omega_p + \sigma) + d\omega_s\ (i - 1/2) + i\sigma]}{[(A^*_s)^{1/2} - 2\delta^*_s]^2\ .\ K}\ \rho \qquad \text{(A-16)}$$

where n_s is the number of secondary layers and the total length being the sum of the lengths of the layers.

Primary Capacitance C_o:

The calculation must be split into two cases. Case 1 is the occurrence of a single layer of primary turns. Case 2 deals with the use of two or more layers of primary turns.

Case 1:

As noted in the discussion of the model, the value of C_o for this case is the value of the turn to turn capacitance, divided by number of turns. The turn to turn capacitance is given by the following formula:

$$C_t = \frac{k\epsilon_i(2\pi)\ \ (a + \sigma)\ d\omega_p}{2\delta_p} \qquad \text{(A-17)}$$

where k = 0.6.

The empirical factor of 0.6 arises from the fact that the windings are fabricated in such a manner as to allow adjacent turns to contact along the inner circumference of the toroid and then diverge to the outer circumference. The divergence between turns is assumed to be symmetrical around the layer.

Therefore, the value of C_o for Case 1 is:

$$C_o = \frac{k}{N_p} \quad \frac{\varepsilon_i \ (2\pi) \ (a + \sigma) \ d\omega_p}{2\delta_p} \qquad \text{(A-18)}$$

Case 2:

We have previously determined that the value of C_o for this case is given by the series sum of the interlayer capacitances plus the turn to turn capacitance divided by the number of turns per layer. In practice, the contribution of the turn to turn capacitance is negligible and the value of C_o becomes the series sum of the interlayer capacitances. The value of the j^{th} interlayer capacitance is given by the following formula.

$$C_j = \frac{\varepsilon_i \ 4\pi^2 \ r \ a_j}{\sigma + 2\delta_p} \qquad \text{(A-19)}$$

where

$$a_j = a + j \ (d\omega_p + \sigma) \qquad \text{(A-20)}$$

Therefore,

$$C_j = \frac{\varepsilon_i \ 4\pi^2 \ r[a + j \ (d\omega_p + \sigma)]}{\sigma + 2\delta_p} \qquad \text{(A-21)}$$

where ε_i is the permittivity of the dielectrics of σ and δ_p which, usually, are very nearly the same.

From the above calculations, it follows that C_o is given by:

$$C_o = \left[\sum_{j=1}^{n_p = i} \frac{\sigma + 2\delta_p}{\varepsilon_i \ 4\pi^2 \ r[a + j \ (d\omega_p + \sigma)]} \right]^{-1} \qquad \text{(A-22)}$$

The Secondary Capacitance C_2:

The same formula holds for C_2 , with the value of a_i being given by:

Case 1:

$$a_i = a + n_p d\omega_p + (n_p + 1)\sigma \qquad \text{(A-23)}$$

Therefore,

$$C_2 = \frac{k}{N_s} \frac{\varepsilon_i [(a + n_p d_p + (n_p + 1)\sigma) d\omega_s]}{2\delta_s} \qquad \text{(A-24}$$

Case 2:

$$a_i = a + n_p (d\omega_p + \sigma) + i (d\omega_s + \sigma) \qquad \text{(A-25)}$$

Therefore,

$$C_2 = \left[\sum_{i=1}^{n_s=1} \frac{\sigma + 2\delta_s}{4\pi^2 \varepsilon_i r [a + n_p (d\omega_p + \sigma) + i(d\omega_s + \sigma)]} \right]^{-1} \qquad \text{(A-26)}$$

The Intercoupling Capacitance C_1:

The value of this capacitance is equal to the value of the interlayer capacitance between the last primary layer and the first secondary layer divided by two. This distributes the coupling capacitance symmetrically between the end points of the primary and secondary windings.

$$C_1 = \frac{2\pi^2 \varepsilon_i r [a + n_p (d\omega_p + \sigma)]}{\sigma + 2\delta_p} \qquad \text{(A-27)}$$

Calculation of the Primary and Secondary Inductance

Several methods of calculating the inductance of a multilayer toroidal winding have been experimentally tested. All of these methods were based on the straight forward calculation of the inductance of a single layer of toroidal windings. The approach given below has been found to be the most consistent with experimental results. Calculations made by this formulation underestimate the measured value of inductance by about five percent.

The flux created by a single layer of turns on a toroid of radius r, and a net cross sectional radius a_j may be expressed as:

$$\phi_j = \mu_o N_j I [r - (r^2 - a_j^2)^{1/2}] \qquad \text{(A-28)}$$

Therefore the total flux produced by n layers of windings is given by the following summation.

$$\phi = \sum_{j=1}^{n} \phi_j = \sum_{j=1}^{n} \mu_o N_j I [r - (r^2 - a_j^2)^{1/2}] \qquad \text{(A-29)}$$

Now the assumption is made that all the flux created by the combined layers links all the turns. Defining inductance as the total number of flux linkages divided by the current, the following result obtains:

$$L = \left(\sum_{M=1}^{n} N_M\right)\left(\sum_{j=1}^{n} \mu_o N_j [r - (r^2 - a_j^2)^{1/2}]\right) \qquad \text{(A-30)}$$

This result immediately implies the following relations for L_1 and L_2.

$$L_1 = \sum_{M=1}^{n_p} N_M \sum_{j=1}^{n_p} \mu_o N_j [r - (r^2 - a_j^2)^{1/2}] \qquad \text{(A-31)}$$

$$L_2 = \sum_{M=1}^{n_s} N_M \sum_{j=1}^{n_s} \mu_o N_j [r - (r^2 - a_j^2)^{1/2}] \qquad \text{(A-32)}$$

where previous definitions of a_j for the primary and secondary layers are used here.

Calculation of M, the Mutual Inductance:

The calculation of the value of M is based on the following assumptions.

(1) The coupling is symmetrical between the two windings.

(2) All the flux created by a current in the primary winding links all the turns of the secondary.

Assumption (1) is susceptible to a rigorous proof and assumption (2) has been found to yield good agreement with

experiment. Using these assumptions, we obtain the following result.

$$L_1 = \left(\sum_{j=1}^{n_p} N_j\right)\left(\sum_{j=1}^{n_p} \mu_o N_j \left[r - (r^2 - a_j^2)^{1/2}\right]\right) \qquad \text{(A-33)}$$

Φ_{21} = flux existing in the secondary due to primary current.

$$\Phi_{21} = \sum_{j=1}^{n_p} I_1 \mu_o N_j \left[r - (r^2 - a_j^2)^{1/2}\right] \qquad \text{(A-34)}$$

Φ_{21} = Flux linkages of secondary

$$\Phi_{21} = \sum_{i=1}^{n_s} N_i \Phi_{21} \qquad \text{(A-35)}$$

Hence:

$$M = \frac{\sum_{i=1}^{n_s} N_i}{\sum_{j=1}^{n_p} N_j} L_1 \qquad \text{(A-36)}$$

$$M = (\text{Turns Ratio})\ L_1 \qquad \text{(A-37)}$$

Appendix B

LAPLACE ANALYSIS OF THE MODEL

Using the conventions shown in Figure B-1 and assuming zero initial conditions in all cases, the following equations describe the behavior of the model. An abbreviated notation for each equation is also given for convenience in later manipulations. "s" is the Laplace Transform complex frequency.

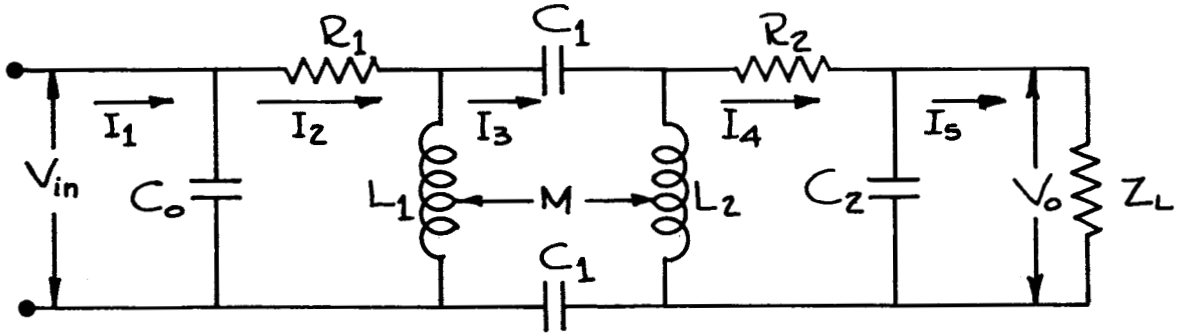

Figure B-1: The Proposed Transformer with Resistive Loading.

Loop 1:

$$V(s) = \frac{I_1(s)}{C_o} s^{-1} - \frac{I_2(s)}{C_o} s^{-1} \qquad \text{(B-1a)}$$

$$V(s) = a_{11} I_1(s) + a_{12} I_2(s) \qquad \text{(B-1b)}$$

Loop 2:

$$0 = -\frac{I_1(s)}{C_o} s^{-1} + \left(\frac{1}{C_0} s^{-1} + R_1 + L_1 s\right) I_2(s) + (M - L_1) sI_3(s) - Ms I_4(s) \qquad \text{(B-2a)}$$

$$0 = a_{21} I_1(s) + a_{22} I_2(s) + a_{23} I_3(s) + a_{24} I_4(s) \qquad \text{(B-2b)}$$

Loop 3;

$$0 = (M - L_1) sI_2(s) + \left[L_1 + L_2 - 2M) s + \frac{2}{C_o} s^{-1}\right] I_3(s) + (M - L_2) sI_4(s) \qquad \text{(B-3a)}$$

$$0 = a_{32}\, I_2(s) + a_{33}\, I_3(s) + a_{34}\, I_4(s) \qquad \text{(B-3b)}$$

Loop 4:

$$0 = -Ms\, I_2(s) + (M - L_2)s\, I_3(s) + \left(L_2 s + R_2 + \frac{s^{-1}}{C_2}\right) I_4(s) \frac{-I_5(s)}{C_2}\, s^{-1} \qquad \text{(B-4a)}$$

$$0 = a_{42}\, I_2(s) + a_{43}\, I_3(s) + a_{44}\, I_4(s) + a_{45}\, I_5(s) \qquad \text{(B-4b)}$$

Loop 5:

$$0 = -\frac{I_4(s)}{C_2}\, s^{-1} + \left(Z_L + \frac{s^{-1}}{C_2}\right) I_5(s) \qquad \text{(B-5a)}$$

$$0 = a_{54}\, I_4(s) + a_{55}\, I_5(s) \qquad \text{(B-5b)}$$

Using the abbreviated notation given above, the following system determinant may be written .

$$\Delta = \begin{vmatrix} a_{11} & a_{12} & 0 & 0 & 0 \\ a_{21} & a_{22} & a_{23} & a_{24} & 0 \\ 0 & a_{32} & a_{33} & a_{34} & 0 \\ 0 & a_{42} & a_{43} & a_{44} & a_{45} \\ 0 & 0 & 0 & a_{54} & a_{55} \end{vmatrix} \qquad \text{(B-6)}$$

Application of standard determinant theory yields the following value for Δ .

$$\Delta = \frac{1}{\beta_5}\left(\beta_4\, s^4 + \beta_3\, s^3 + \beta_2\, s^2 + \beta_1\, s + \beta_0\right) \qquad \text{(B-7)}$$

where

$$\beta_5 = s^3\, C_1\, C_o\, C_2. \qquad \text{(B-8a)}$$

$$\beta_4 = Z_L\, C_1\, C_2\, (L_1\, L_2 - M^2)\, (R_1 + R_2) \qquad \text{(B-8b)}$$

$$\beta_3 = Z_L\, (2C_2 + C_1)(L_1\, L_2 - M^2) + C_1 C_2\, Z_L\, R_1\, R_2\, (L_1 + L_2 - 2M)$$

$$+ C_1 (R_1 + R_2) (L_1 L_2 - M^2) \qquad \text{(B-8c)}$$

$$\beta_2 = Z_L R_1 C_1 (L_1 + L_2 - 2M) + 2Z_L C_2 (L_2 R_1 + R_2 L_1) + 2(L_1 L_2 - M^2) + R_1 R_2 C_1 (L_1 + L_2 - 2M) \qquad \text{(B-8d)}$$

$$\beta_1 = 2 Z_L C_2 (R_1 R_2 + L_1/C_2) + 2(R_1 L_2 + R_2 L_1) \qquad \text{(B-8e)}$$

$$\beta_o = 2R_1 (Z_L + R_2) \qquad \text{(B-8f)}$$

Note that Z_L is assumed to be purely resistive.

Determination of the Input Impedance

The input impedance is defined to be the ratio of the input voltage, V(s) , to the input current, $I_1(s)$.

i.e.

$$Z_{in} = \frac{V(s)}{I_1(s)} \qquad \text{(B-9)}$$

However:

$$I_1(s) = \frac{\Delta_1(s)}{\Delta} \qquad \text{(B-10)}$$

where:

$$\Delta_1 = \begin{vmatrix} V(s) & a_{12} & 0 & 0 & 0 \\ 0 & a_{22} & a_{23} & a_{24} & 0 \\ 0 & a_{32} & a_{33} & a_{34} & 0 \\ 0 & a_{42} & a_{43} & a_{44} & a_{45} \\ 0 & 0 & 0 & a_{54} & a_{55} \end{vmatrix} \qquad \text{(B-11)}$$

The solution of this determinant yields the following equation for Δ_1.

$$\Delta_1 = \frac{V(s)}{\lambda_6} (\lambda_5 s^5 + \lambda_4 s^4 + \lambda_3 s^3 + \lambda_2 s^2 + \lambda_1 s + \lambda_o) \qquad \text{(B-12)}$$

where:

$$\lambda_6 = s^3 C_0 C_1 C_2 \qquad \text{(B-13a)}$$

$$\lambda_5 = C_o C_1 C_2 Z_L (R_1 + R_2) (L_1 L_2 - M^2) \qquad \text{(B-13b)}$$

$$\lambda_4 = Z_L(C_1 C_2 + 2C_o C_2 + C_1 C_o) (L_1L_2 - M^2) + Z_L C_o C_1 C_2 R_1 R_2 (L_1 + L_2 - 2M) + C_1 C_o (R_1 + R_2)(L_1 L_2 - M^2) \qquad \text{(B-13c)}$$

$$\lambda_3 = C_1 Z_L(C_2R_2 + C_oR_1)(L_1 + L_2 - 2M) + 2Z_L C_oC_2 (R_1L_2 + R_2L_1) + (C_1 + 2 C_o) (L_1 L_2 - M^2) + R_1R_2C_1C_o (L_1 + L_2 - 2M) \qquad \text{(B-13d)}$$

$$\lambda_2 = Z_L C_1 (L_1 + L_2 - 2M) + 2Z_L C_o C_2 \left(R_1 R_2 + \frac{L_1}{C_2} + \frac{L_2}{C_o}\right) + R_2 C_1 (L_1 + L_2 - 2M) + 2C_o (R_1 L_2 + R_2 L_1) \qquad \text{(B-13e)}$$

$$\lambda_1 = 2Z_L (R_2 C_2 + R_1 C_o) + 2(C_o R_1 R_2 + L_2) \qquad \text{(B-13f)}$$

$$\lambda_o = 2(Z_L + R_2) \qquad \text{(B-13g)}$$

Therefore:

$$Z_{in}(s) = \frac{V(s)}{I_1(s)} = \frac{V(s)\,\Delta(s)}{\Delta_1(s)} \qquad \text{(B-14a)}$$

$$Z_{in}(s) = \frac{\left(\beta_4 s^4 + \beta_3 s^3 + \beta_2 + \beta_1 s + \beta_0\right) \lambda_6}{\left(\lambda_5 s^5 + \lambda_4 s^4 + \lambda_3 s^3 + \lambda_2 s^2 + \lambda_1 s + \lambda_0\right)\beta_5} \qquad \text{(B-14b)}$$

The substitution $s = j\omega$ is made and rationalization yields the following result.

$$Z_{in}(j\omega) = \frac{P_1 P_3 + P_2 P_4}{P_3^2 + P_4^2} + j \frac{P_2 P_3 - P_1 P_4}{P_3^2 + P_4^2} \qquad \text{(B-14c)}$$

$$= Q_1 + j\,Q_2 \qquad \text{(B-14d)}$$

where

$$P_1 = \beta_4\omega^4 - \beta_2\omega^2 + \beta_0 \qquad \text{(B-15a)}$$

$$P_2 = \beta_1\omega - \beta_3\omega^3 \qquad \text{(B-15b)}$$

$$P_3 = \lambda_4\omega^4 - \lambda_2\omega^2 + \lambda_0 \qquad \text{(B-15c)}$$

$$P_4 = \lambda_5\omega^5 - \lambda_3\omega^3 + \lambda_1\omega \qquad \text{(B-15d)}$$

Therefore, we have the magnitude of Z_{in} as;

$$|Z_{in}| = (Q_1^2 + Q_2^2)^{1/2} \qquad \text{(B-16)}$$

and the phase angle of Z_{in} as:

$$\psi(Z_{in}) = \tan^{-1}(Q_2/Q_1) \qquad \text{(B-17)}$$

Determination of the Voltage Transfer Function:

Defining the transfer function as the ratio of the load voltage to the input voltage, we have the following results.

$$G(s) = \frac{V_o(s)}{V(s)} \qquad \text{(B-18)}$$

$$V_o(s) = I_5(s)\,Z_L = \frac{\Delta_5(s)\,Z_L}{\Delta(s)} \qquad \text{(B-19)}$$

where

$$\Delta_5(s) = \begin{vmatrix} a_{11} & a_{12} & 0 & 0 & V(s) \\ a_{21} & a_{22} & a_{23} & a_{24} & 0 \\ 0 & a_{32} & a_{33} & a_{34} & 0 \\ 0 & a_{42} & a_{43} & a_{44} & 0 \\ 0 & 0 & 0 & a_{54} & 0 \end{vmatrix} \qquad \text{(B-20)}$$

Solution of the above determinant yields:

$$\Delta_5(s) = \frac{V(s)}{T_4} \; T_3 \; s^3 + T_1 \; s \tag{B-21}$$

Defining:

$$T_4 = s^3 \; C_o \; C_1 \; C_2 \tag{B-22a}$$

$$T_3 = C_1 \; (L_1 \; L_2 - M_2) \tag{B-22b}$$

$$T_1 = 2M \tag{B-22c}$$

Hence, we have:

$$I_5(s) = V(s) \; \frac{T_3 \; s^3 + T_1 \; s}{\beta_4 \; s^4 + \beta_3 \; s^3 + \beta_2 \; s^2 + \beta_1 \; s^1 + \beta_o} \tag{B-23}$$

Therefore:

$$V_o(s) = Z_L V(s) \; \frac{T_3 \; s^3 + T_1 \; s}{\beta_4 \; s^4 + \beta_3 \; s^3 + \beta_2 \; s^2 + \beta_1 \; s + \beta_o} \tag{B-24}$$

These results yield the following result for G(s)

$$G(s) = \frac{Z_L \; T_3 \; s^3 + Z_L \; T_1 \; s}{\beta_4 \; s^4 + \beta_3 \; s^3 + \beta_2 \; s^2 + \beta_1 \; s + \beta_o} \tag{B-25}$$

Substitution of $s = j\omega$ and rationalization yields the following equations:

$$G(j\omega) = \frac{S_1 \; P_2}{P_1^2 + P_2^2} + j \; \frac{S_1 \; P_1}{P_1^2 + P_2^2} = Z_1 + j \; Z_2 \tag{B-26}$$

where:

$$S_1 = Z_L T_1 \omega - Z_L T_3 \omega^3 \tag{B-27}$$

Reducing eq. (B-26) we obtain:

$$G(j\omega) = [Z_1^2 + Z_2^2]^{1/2} \qquad \text{(B-28a)}$$

$$\Theta(G) = \tan^{-1}(Z_2/Z_1) \qquad \text{(B-28b)}$$

Determination of the efficiency:

Using the standard definition of efficiency, and the relations between the quantities derived above, the following results are obtained.

$$E = P_{out}/P_{in} \qquad \text{(B-29)}$$

$$P_{in} = \frac{|V|^2}{|Z_{in}|} \cos [\psi(Z_{in})] \qquad \text{(B-30)}$$

$$P_{out} = \frac{|V_o|^2}{Z_L} \qquad \text{(B-31)}$$

Therefore:

$$E = \frac{|V_o|^2 \quad |Z_{in}|}{|V_{in}|^2 \quad Z_L \cos [\psi(Z_{in})]} \qquad \text{(B-32)}$$

However:

$$|V_o| = |G| \; |V_{in}| \qquad \text{(B-33)}$$

Therefore:

$$E = \frac{|G|^2 \quad |Z_{in}|}{Z_L \cos [\psi(Z_{in})]} \qquad \text{(B-34)}$$

Determination of the Resonant Frequencies

The resonant frequencies are determined by equating the imaginary part of $Z_{in}(j\omega)$ to zero and solving the resulting polynomial for its roots.

$$I_m [Z(j\omega)] = \frac{P_2P_3 - P_1P_4}{P_3^2 + P_4^2}$$

Therefore, we need consider only the expression

$$P_2P_3 - P_1P_4 = 0$$

Using the definitions of the P's given previously, we obtain, after some manipulation:

$$R_1\omega^8 + R_2\omega^7 + R_3\omega^6 + R_4\omega^5 + R_5\omega^4 + R_6\omega^3 + R_7\omega^2 + R_8\omega^1 + R_9 = 0$$

Where:

$R_1 = \lambda_5\beta_4$

$R_2 = 0.0$

$R_3 = \beta_3\lambda_4 - \beta_4\lambda_3 - \beta_2\lambda_5$

$R_4 = 0.0$

$R_5 = \beta_4\lambda_1 + \beta_2\lambda_3 - \beta_3\lambda_2 - \beta_1\lambda_4 + \beta_0\lambda_5$

$R_6 = 0.0$

$R_7 = \beta_1\lambda_2 + \beta_3\lambda_0 - \beta_2\lambda_1 - \beta_0\lambda_3$

$R_8 = 0.0$

$R_9 = \beta_0\lambda_1 - \beta_1\lambda_0$

Clearly, this equation contains only the even powers of ω, and a constant. The zero valued coefficients are defined for use.in the computer solution of the equation.

In general, the equation given above must be scaled to avoid exceeding the limits of number size within the computer.

Appendix C

PARTIAL DERIVATIVES OF THE IMPORTANT CIRCUIT FUNCTIONS WITH RESPECT TO THE CIRCUIT PARAMETERS

In order to partially adapt the model analysis for design work, it is desirable to have information concerning the rates of change of the critical functions with respect to the individual parameters of the equivalent circuit. To facilitate the derivation of these relations, the following definitions are made.

$$e_1 = C_o \tag{C-1a}$$

$$e_2 = R_1 \tag{C-1b}$$

$$e_3 = L_1 \tag{C-1c}$$

$$e_4 = M \tag{C-1d}$$

$$e_5 = C_1 \tag{C-1e}$$

$$e_6 = L_2 \tag{C-1f}$$

$$e_7 = R_2 \tag{C-1g}$$

$$e_8 = C_2 \tag{C-1h}$$

$$e_9 = Z_L \tag{C-1k}$$

Rates of Change of Z_{in}:

Differentiating equation (B-16), we obtain:

$$\frac{\partial Z_{in}}{\partial e_j} = \frac{Q_1}{(Q_1^2 + Q_2^2)^{1/2}} \frac{\partial Q_1}{\partial e_j} + \frac{Q_2}{[Q_1^2 + Q_2^2]^{1/2}} \frac{\partial Q_2}{\partial e_j} \tag{C-2}$$

Referring to eqs. (B-14c) and (B-14d), it follows that

$$\frac{\partial Q_1}{\partial e_j} = \frac{\partial Q_1}{\partial P_1} \frac{\partial P_1}{\partial e_j} + \frac{\partial Q_1}{\partial P_2} \frac{\partial P_2}{\partial e_j} + \frac{\partial Q_1}{\partial P_3} \frac{\partial P_3}{\partial e_j} + \frac{\partial Q_1}{\partial P_4} \frac{\partial P_4}{\partial e_j} \tag{C-3}$$

Also:

$$\frac{\partial Q_1}{\partial P_1} = \frac{P_3}{P_3^2 + P_4^2} \tag{C-4}$$

$$\frac{\partial Q_1}{\partial P_2} = \frac{P_4}{P_3^2 + P_4^2} \tag{C-5}$$

$$\frac{\partial Q_1}{\partial P_3} = \frac{P_1(P_4^2 - P_3^2) - 2P_2P_3P_4}{(P_3^2 + P_4^2)^2} \tag{C-6}$$

$$\frac{\partial Q_1}{\partial P_4} = \frac{P_2(P_3^2 - P_4^2) - 2P_1P_3P_4}{(P_3^2 + P_4^2)^2} \tag{C-7}$$

and

$$\frac{\partial Q_2}{\partial P_1} = -\frac{\partial Q_1}{\partial P_2} \tag{C-8}$$

$$\frac{\partial Q_2}{\partial P_2} = \frac{\partial Q_1}{\partial P_1} \tag{C-9}$$

$$\frac{\partial Q_2}{\partial P_3} = \frac{\partial Q_1}{\partial P_4} \tag{C-10}$$

$$\frac{\partial Q_2}{\partial P_4} = \frac{\partial Q_1}{\partial P_3} \tag{C-11}$$

From eqs. (B-15a) - (B-15d) the following may be obtained:

$$\frac{\partial P_1}{\partial e_j} = \omega^4 \frac{\partial \beta_4}{\partial e_j} - \omega^2 \frac{\partial \beta_2}{\partial e_j} + \frac{\partial \beta_0}{\partial e_j} \tag{C-12}$$

$$\frac{\partial P_2}{\partial e_j} = \omega \frac{\partial \beta_1}{\partial e_j} - \omega^3 \frac{\partial \beta_3}{\partial e_j} \tag{C-13}$$

$$\frac{\partial P_3}{\partial e_j} = \omega^4 \frac{\partial \lambda_4}{\partial e_j} - \omega^2 \frac{\partial \lambda_2}{\partial e_j} + \frac{\partial \lambda_0}{\partial e_j} \tag{C-14}$$

$$\frac{\partial P_4}{\partial e_j} = \omega^5 \frac{\partial \lambda_5}{\partial e_j} - \omega^3 \frac{\partial \lambda_3}{\partial e_j} + \omega \frac{\partial \lambda_1}{\partial e_j} \tag{C-15}$$

Combining the results of eqs. (C-1a)-(C-15), the rates of change of the magnitude of the input impedance are:

$$\frac{\partial |Z_{in}|}{\partial e_j} = \frac{1}{(Q_1^2 + Q_2^2)^{1/2}} \left\{ Q_1 \left[\frac{P_3}{P_3^2 + P_4^2} \left(\omega^4 \frac{\partial \beta_4}{\partial e_j} - \omega^2 \frac{\partial \beta_2}{\partial e_j} + \frac{\partial \beta_0}{\partial e_j} \right) \right. \right.$$

$$\left. + \frac{P_4}{P_3^2 + P_4^2} \left(\omega \frac{\partial \beta_1}{\partial e_j} - \omega^3 \frac{\partial \beta_3}{\partial e_j} \right) + \left(\frac{P_4^2 P_1 - P_1 P_3^2 - 2 P_2 P_3 P_4}{(P_3^2 + P_4^2)^2} \right) \right.$$

$$\left(\omega^4 \frac{\partial \lambda_4}{\partial e_j} - \omega^2 \frac{\partial \lambda_2}{\partial e_j} + \frac{\partial \lambda_0}{\partial e_j}\right) + \left(\frac{P_3^2 P_2 - P_2 P_4^2 - 2 P_1 P_3 P_4}{(P_3^2 + P_4^2)^2}\right)$$

$$\left(\omega^5 \frac{\partial \lambda_5}{\partial e_j} - \omega^3 \frac{\partial \lambda_3}{\partial e_j} + \omega \frac{\partial \lambda_1}{\partial e_j}\right)\Bigg] + Q_2 \Bigg[\left(\frac{-P_4}{P_3^2 + P_4^2}\right)$$

$$\left(\omega^4 \frac{\partial \beta_4}{\partial e_j} - \omega^2 \frac{\partial \beta_2}{\partial e_j} + \frac{\partial \beta_0}{\partial e_j}\right) + \frac{P_3}{P_3^2 + P_4^2} \left(\omega \frac{\partial \beta_1}{\partial e_j} - \omega^3 \frac{\partial \beta_3}{\partial e_j}\right)$$

$$+ \left(\frac{P_2 P_4^2 + 2 P_1 P_3 P_4 - P_3^2 P_2}{(P_3^2 + P_4^2)^2}\right)\left(\omega^4 \frac{\partial \lambda_4}{\partial e_j} - \omega^2 \frac{\partial \lambda_2}{\partial e_j} + \frac{\partial \lambda_0}{\partial e_j}\right)$$

$$+ \left(\frac{P_4^2 P_1 - P_1 P_3^2 - 2 P_2 P_3 P_4}{(P_3^2 + P_4^2)^2}\right)\left(\omega^5 \frac{\partial \lambda_5}{\partial e_j} - \omega^3 \frac{\partial \lambda_3}{\partial e_j} + \omega \frac{\partial \lambda_1}{\partial e_j}\right)\Bigg]\Bigg\} \tag{C-16}$$

Rates of Change of $|G_v|$:

Differentiating eq. (B-28a) gives:

$$\frac{\partial |G_v|}{\partial e_j} = \frac{1}{(Z_1^2 + Z_2^2)^{\frac{1}{2}}} \left[Z_1 \frac{\partial Z_1}{\partial e_j} + Z_2 \frac{\partial Z_2}{\partial e_j}\right] \tag{C-17}$$

From eq. (B-26), we obtain:

$$\frac{\partial Z_1}{\partial e_j} = \frac{\partial Z_1}{\partial S_1}\frac{\partial S_1}{\partial e_j} + \frac{\partial Z_1}{\partial P_1}\frac{\partial P_1}{\partial e_j} + \frac{\partial Z_1}{\partial P_2}\frac{\partial P_2}{\partial e_j} \qquad \text{(C-18)}$$

Differentiation of eq. (B-27) yields:

$$\frac{\partial S_1}{\partial e_j} = Z_L\left(\omega \frac{\partial T_1}{\partial e_j} - \omega^3 \frac{\partial T_3}{\partial e_j}\right) \qquad \text{(C-19)}$$

Also, from eq. (B-26), it follows:

$$\frac{\partial Z_1}{\partial S_1} = \frac{P_2}{P_1^2+P_2^2} \qquad \text{(C-20)}$$

$$\frac{\partial Z_1}{\partial P_1} = \frac{-2S_1P_2P_1}{(P_1^2+P_2^2)^2} \qquad \text{(C-21)}$$

$$\frac{\partial Z_1}{\partial P_2} = \frac{-2S_1P_2^2}{(P_1^2+P_2^2)^2} + \frac{S_1}{(P_1^2+P_2^2)} \qquad \text{(C-22)}$$

$$\frac{\partial Z_2}{\partial S_1} = \frac{P_1}{P_1^2+P_2^2} \qquad \text{(C-23)}$$

$$\frac{\partial Z_2}{\partial P_1} = \frac{-2S_1P_1^2}{(P_1^2+P_2^2)^2} + \frac{S_1}{(P_1^2+P_2^2)} \qquad \text{(C-24)}$$

$$\frac{\partial Z_2}{\partial P_2} = \frac{-2 S_1 P_2 P_1}{(P_1^2 + P_2^2)^2} \qquad \text{(C-25)}$$

We now combine the results of eqs. (C-17)-(C-25) with eqs. (C-12) and (C-15) and obtain the following:

$$\frac{\partial |G_V|}{\partial e_j} = \frac{1}{(Z_1^2 + Z_2^2)^{1/2}} \left\{ Z_1 \left[\frac{P_2 Z_L}{P_1^2 + P_2^2} \left(\omega \frac{\partial T_1}{\partial e_j} - \omega^3 \frac{\partial T_3}{\partial e_j} \right) \right.\right.$$

$$+ \left(\frac{-2 S_1 P_1 P_2}{(P_1^2 + P_2^2)^2} \right) \left(\omega^4 \frac{\partial \beta_4}{\partial e_j} - \omega^2 \frac{\partial \beta_2}{\partial e_j} + \frac{\partial \beta_0}{\partial e_j} \right)$$

$$\left. + \left(\frac{S_1}{P_1^2 + P_2^2} - \frac{2 S_1 P_2^2}{(P_1^2 + P_2^2)^2} \right) \left(\omega \frac{\partial \beta_1}{\partial e_j} - \omega^3 \frac{\partial \beta_3}{\partial e_j} \right) \right]$$

$$+ Z_2 \left[\frac{P_1 Z_L}{P_1^2 + P_2^2} \left(\omega \frac{\partial T_1}{\partial e_j} - \omega^3 \frac{\partial T_3}{\partial e_j} \right) + \left(\frac{S_1}{P_1^2 + P_2^2} - \frac{2 S_1 P_1^2}{(P_1^2 + P_2^2)^2} \right) \right.$$

$$\left. \left. \left(\omega^4 \frac{\partial \beta_4}{\partial e_j} - \omega^2 \frac{\partial \beta_2}{\partial e_j} + \frac{\partial \beta_0}{\partial e_j} \right) - \left(\frac{2 S_1 P_1 P_2}{(P_1^2 + P_2^2)^2} \right) \left(\omega \frac{\partial \beta_1}{\partial e_j} - \omega^3 \frac{\partial \beta_3}{\partial e_j} \right) \right] \right\}$$

(C-26)

Rates of Change of $\psi(Z_{in})$:

From equation (B-17) we see that;

$$\psi(Z_{in}) = \tan^{-1}\left(\frac{Q_2}{Q_1}\right) = \tan^{-1}\left(\frac{P_2P_3 - P_1P_4}{P_1P_3 + P_2P_4}\right) = \tan^{-1}(v) \tag{C-27}$$

Hence:

$$\frac{\partial\psi}{\partial P_i} = \frac{1}{1+v^2}\frac{\partial v}{\partial P_i} \qquad (i = 1,2,3,4) \tag{C-28}$$

From equation (C-26), it follows that:

$$\frac{\partial v}{\partial P_1} = \frac{-P_2(P_3^2+P_4^2)}{(P_1P_3+P_2P_4)^2} \tag{C-29}$$

$$\frac{\partial v}{\partial P_2} = \frac{P_1(P_3^2+P_4^2)}{(P_1P_3+P_2P_4)^2} \tag{C-30}$$

$$\frac{\partial v}{\partial P_3} = \frac{P_4(P_1^2+P_2^2)}{(P_1P_3+P_2P_4)^2} \tag{C-31}$$

$$\frac{\partial v}{\partial P_4} = \frac{-P_3(P_1^2+P_2^2)}{(P_1P_3+P_2P_4)^2} \tag{C-32}$$

Therefore, combining equations (C-28)-(C-31), with eqs. (C-12)-(C-15), and (C-27), we have for the rates of change of $\psi(Z_{in})$:

$$\frac{\partial\psi(Z_{in})}{\partial e_j} = \left[(P_2P_3 - P_1P_4)^2 + (P_1P_3 + P_2P_4)^2\right]^{-1}$$

$$\left\{\left(-P_2(P_3^2+P_4^2)\right)\left(\omega^4\frac{\partial\beta_4}{\partial e_j} - \omega^2\frac{\partial\beta_2}{\partial e_j} + \frac{\partial\beta_0}{\partial e_j}\right) + \left(P_1(P_3^2+P_4^2)\right)\right.$$

$$\left(\omega\frac{\partial\beta_1}{\partial e_j} - \omega^3\frac{\partial\beta_3}{\partial e_j}\right) + \left(P_4(P_1^2+P_2^2)\right)\left(\omega^4\frac{\partial\lambda_4}{\partial e_j} - \omega^2\frac{\partial\lambda_2}{\partial e_j} + \frac{\partial\lambda_0}{\partial e_j}\right)$$

$$\left.-\left(P_3(P_1^2+P_2^2)\right)\left(\omega^5\frac{\partial\lambda_5}{\partial e_j} - \omega^3\frac{\partial\lambda_3}{\partial e_j} + \omega\frac{\partial\lambda_1}{\partial e_j}\right)\right\} \qquad \text{(C-33)}$$

Rates of Change of the Efficiency:

Finally, we compute the rates of change of the efficiency by differentiating eq. (B-34).

$$E = \frac{|G_v|^2\,|Z_{in}|}{Z_L\cos[\psi(Z_{in})]} \qquad \text{(C-34)}$$

$$\frac{\partial E}{\partial e_j} = \frac{|G_v|^2}{Z_L\cos[\psi(Z_{in})]}\frac{\partial|Z_{in}|}{\partial e_j} + \frac{2|G_v||Z_{in}|}{Z_L\cos[\psi(Z_{in})]}\frac{\partial|G_v|}{\partial e_j}$$

$$-\frac{|Z_{in}||G_v|^2}{Z_L^2\cos[\psi(Z_{in})]}\frac{\partial Z_L}{\partial e_j} + \frac{|Z_{in}||G_v|^2}{Z_L}\frac{\sin[\psi(Z_{in})]}{\cos^2[\psi(Z_{in})]}\frac{\partial\psi(Z_{in})}{\partial e_j} \qquad \text{(C-35)}$$

Since all the derivatives on the right hand side of equation (C-35) have been defined except $\frac{\partial Z_L}{\partial e_j}$, (which equals zero if $j \neq 9$ and equal 1 if $j = 9$), the rates of change of E are computed as a direct function of the changes of the other critical functions.

Appendix D

ANALYTICAL APPROXIMATION OF THE EXTERNAL MAGNETIC FIELD

In order to obtain an analytical estimate of the magnitude of the leakage field of the distributed winding transformer, the following assumptions are made.

(a) The stray magnetic field of the transformer may be approximated by the magnetic field of a circular current filament having a radius to the outer radius of the transformer, and carrying a current equal to the value of the current flowing in the outermost layer of turns on the transformer.

(b) Calculation of the axial component of magnetic field intensity will suffice for order of magnitude purposes since the total magnetic field intensity reduces to the axial component both along the axis and in the plane of the current filament.

(c) The static (D.C.) field distribution will be the same as the dynamic (A.C.) field distribution. (This is in accord with the model that has been postulated, but not valid near resonance.)

Using the configuration shown in Figure D-1, it is a relatively simple matter to calculate the magnetic field along the axis,[1] which is given by:

$$H_Z = \frac{a^2 I}{2(a^2 + Z^2)^{3/2}} \qquad \text{(D-1)}$$

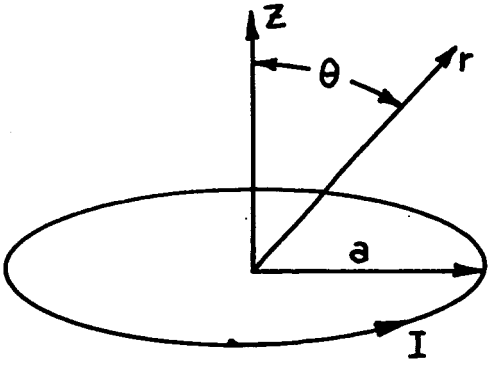

Figure D-1

A general solution for H_Z anywhere in the region may be found in the following way.

(a) H_Z satisfies Laplace's equation in cylindrical coordinates (i.e. $\nabla^2 H_Z = 0$)[1,2]

(b) A solution of Laplace's equation for an arbitrary function ϕ is given by [1]:

$$\phi(r,\theta) = \sum_{m=0} C_m P_m(\cos\theta)\, r^{-(m+1)}$$

where r and θ are usual spherical coordinates and the C_m are constants. $P_m(\cos\theta)$ are the Legendre polynomials of order m.

(c) Furthermore, if ϕ is known along an axis of symmetry, then the solution for ϕ in the region may be obtained by expanding ϕ in a power series and extrapolating to the general solution of Laplace's equation. i.e. If the following convergent series exists,

$$\phi\Big|_{\theta=0} = \sum_{m=0} C_m z^{-(m+1)} \qquad \text{(D-2)}$$

then the general solution for ϕ anywhere in the region is given by:

$$\phi(r,\theta) = \sum_{m=0} C_m P_m(\cos\theta)\, r^{-(m+1)} \qquad \text{(D-3)}$$

Clearly, eq. D-3 reduces to eq. D-2 along the axis where $\theta = 0$, since $P_m(1) = 1$ for all m. Therefore, by the uniqueness theorem, ϕ is the solution for the entire region.

Equation D-1 may be rewritten as follows:

$$H_z = \frac{a^2 I}{2}\, z^{-3}\left(1+[a^2/z^2]\right)^{-3/2} \qquad \text{(D-4)}$$

Now consider the binomial expansion:

$$(1+u)^{-3/2} = 1-(3/2)u+(15/8)u^2-(105/48)u^3$$

$$=\sum_{n=0} \frac{(-1)^n(2n+1)!!\,u^n}{2^n n!}$$

where $(2n+1)!! \equiv (2n+1)(2n-1)(2n-3)(2n-5)\cdots 1$

This series is convergent for $0 \le |u| < 1$

It follows that (D-4) may be expressed as:

$$H_{z_{\theta=0}} = \frac{a^2 I}{2} z^{-3} \sum_{n=0} \frac{(-1)^n(2n+1)!!}{2^n n!} [a/z]^{2n} \qquad \text{(D-5a)}$$

$$=\sum_{n=0} \frac{I(-1)^n(2n+1)!!}{2^n n!}\, a^{2n+2} z^{-(2n+3)} \qquad \text{(D-5b)}$$

Using the following definitions, (D5b) may be given the required form (1) m = 2n + 2

$$(2)\ C_m = \frac{I(-1)^{\frac{m-2}{2}}(m-1)!!\, a^m z^{-(m+1)}}{2^{\frac{m-2}{2}} \left(\frac{m-2}{2}\right)!} \quad \text{for } m = 2,4,6,8,\cdots$$

(3) $C_m = 0$ for m = 0,1,3,5,7, - - - - - - - - - - -

Thus:

$$H_z\Big|_{\theta=0} = \sum_{m=0}^{\infty} C_m P_m(\cos\theta) r^{-(m+1)} \qquad \text{(D-5c)}$$

From the previous discussion, we may immediately conclude that:

$$H_z(r,\theta) = \sum_{m=0}^{\infty} C_m P_m(\cos\theta)\, r^{-(m+1)} \qquad \text{(D-6)}$$

This series converges very rapidly and for a first order approximation to its value, the first four non-zero terms are used. i.e.

$$H_z(r,\theta) = I\left[\frac{a^2}{2} P_2(\cos\theta)\, r^{-3} - \frac{3a^4}{2} P_4(\cos\theta) r^{-5} + \frac{15a^6}{8} P_6(\cos\theta) r^{-7} + \cdots\right] \qquad \text{(D-6a)}$$

Appendix E

SQUARE WAVE OSCILLATOR

This appendix describes a high efficiency square wave oscillator that has been developed to serve as the driver stage for non-magnetic converters.

The schematic diagram in Figure E-1 shows the basic circuit for the oscillator. Essentially, it is a bridge circuit with a transistor in each arm. The base of each transistor is connected to a parallel resistor-capacitor combination and this combination is connected to the collector of the transistor diagonally opposite to it in the bridge. The input is applied to the bridge by grounding point (2) and placing the positive input terminal at point (1). The load is connected between points (3) and (4).

The following discussion demonstrates that this circuit will produce a square wave oscillation across the load R_L that is equal in peak to peak value to twice the magnitude of the applied input voltage. (Neglecting all saturated transistor drops.) Clearly, this necessitates a conducting sequence of transistors A and B alternated with transistors A^1 and B^1.

To begin, assume that transistors A and B are fully on and transistors A^1 and B^1 are completely off. If we again neglect the saturated transistor drops, we find that the load current is equal to the collector current of transistors A and B and is determined by the input voltage divided by the load resistance. Assume a constant input voltage and a fixed value of load resistance, this fixes the load current at a value I_1.

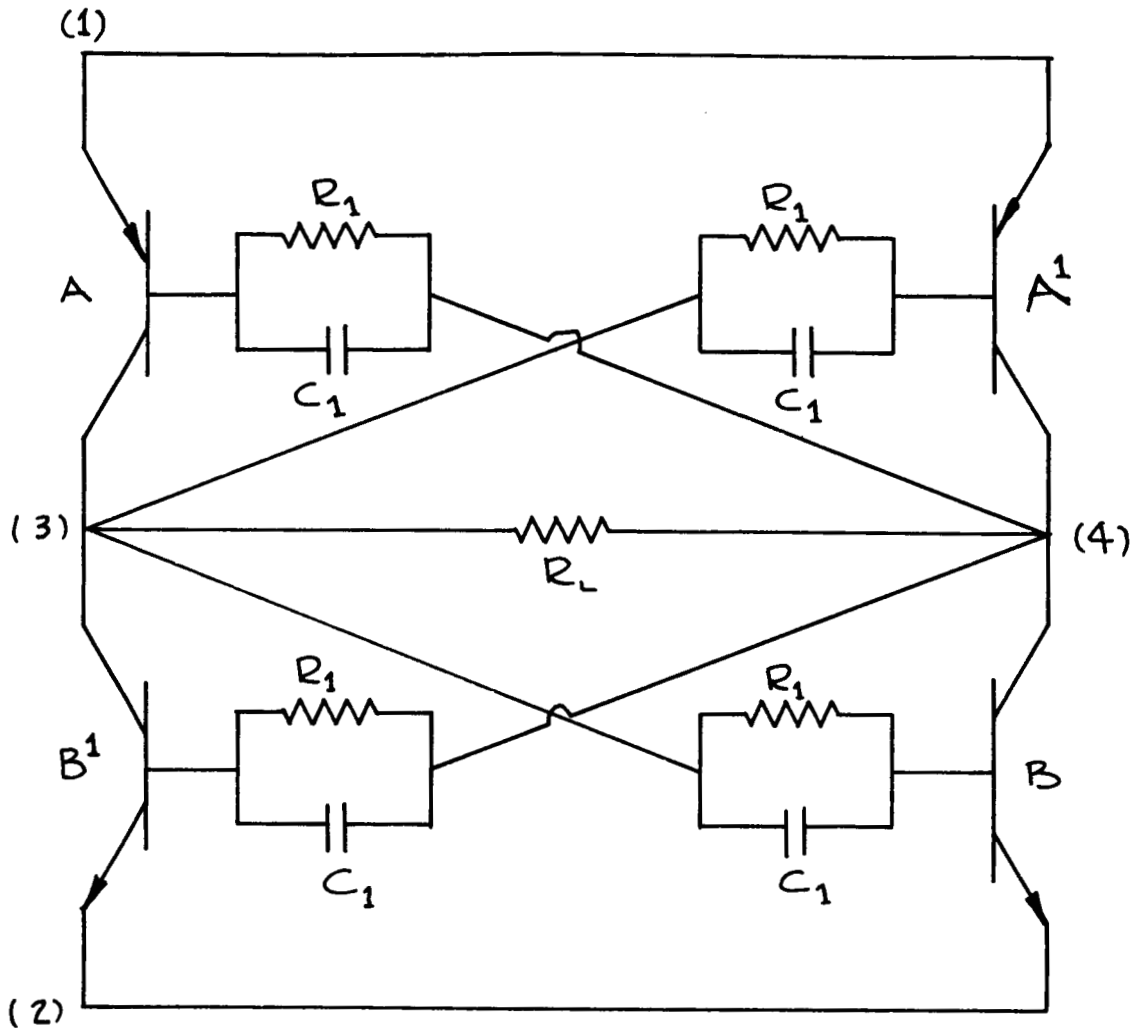

Figure E-1: Basic Oscillator Circuit

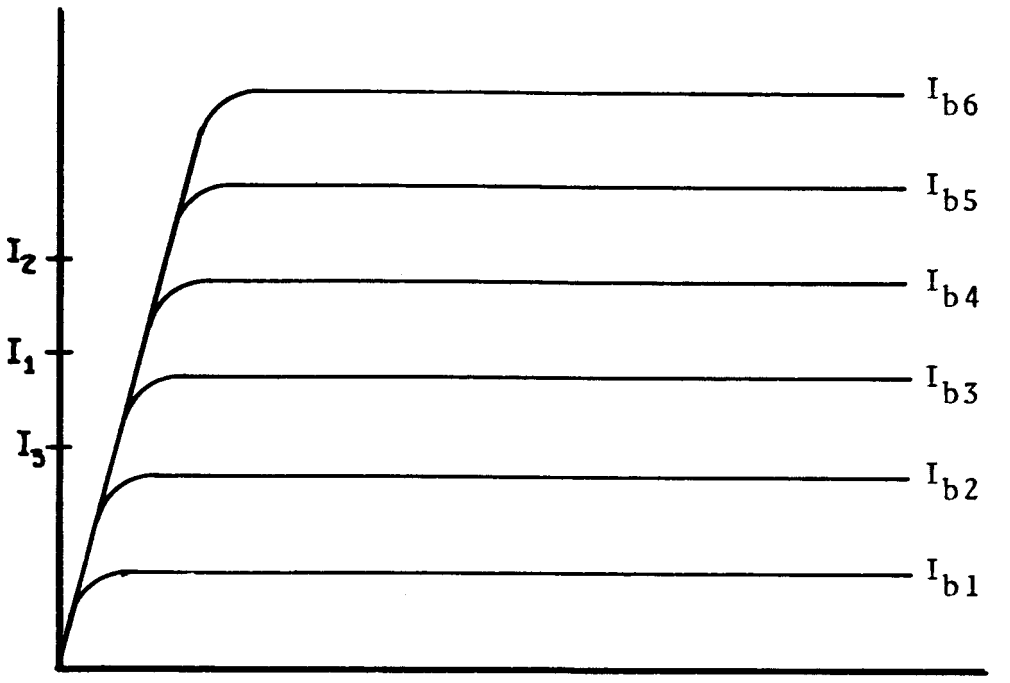

Figure E-2: Transistor Collector Curves

Now refer to the family of collector curves for a transistor as shown in Fig. E-2. The value of collector current I_1 is shown in the figure. Now, consider the base current in the transistors A and B at the instant they become fully on. Since the capacitor voltage in the base circuits of A and B cannot change instantaneously, the initial base current in transistor A will be given by:

$$I_{bi}(A) = \frac{V_{in} - V_s^b - V_{ci}(A)}{R_{be}(A)} \qquad (E\text{-}1)$$

where V_{in} is the input voltage, $V_{ci}(A)$ is the initial voltage across the capacitor in the base of transistor A, and V^b_s is the saturated voltage drop across transistor B. $R_{be}(A)$ is the base-emitter resistance of transistor A.

Similarly, the initial base current in transistor B will be given by:

$$I_{bi}(B) = \frac{V_{in} - V_s^a - V_{ci}(B)}{R_{be}(B)} \qquad (E\text{-}2)$$

where the quantities V_{in}, V^a_s, $- V_{ci}(B)$, are defined as above, with the symbols A and B interchanged. (V^a_s and $V^b_s \ll V_{in}$).

Note that the design must be such that these initial values of base currents are sufficient to maintain transistors A and B in their saturated state while they are delivering a collector current I_1. (i.e., I_{bi} (A) and $I_{bi}(B) > I_{b4}$ shown in Fig. E-2.)

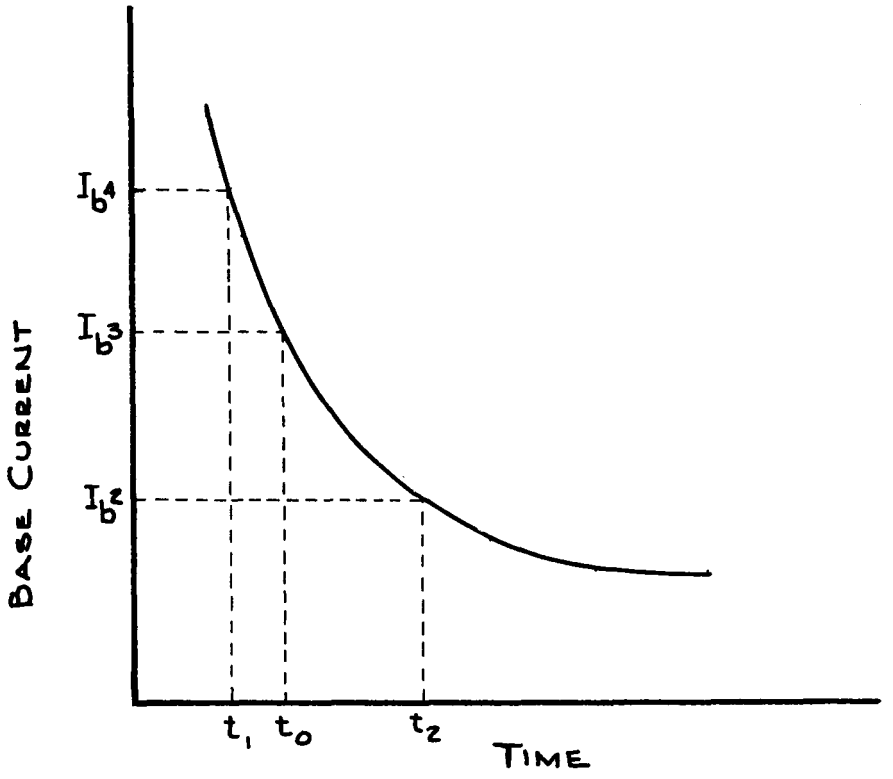

Figure E-3: Base current in Conducting Transistors

The base currents in A and B will decay exponentially as shown in Figure E-3 as the capacitors in the base circuits of A and B begin to charge through their respective base-emitter resistances.

The time constant of this exponential will be determined by the value of C_1 and the respective base-emmitter resistances (where $R_1 >> R_{be}$). As the base currents decay, they will approach the value I_{b3} shown in Figure E-2 and the transistors A and B will start to move out of saturation, causing the V_{ce}

of both transistor A and transistor B to rise sharply. Referring to Figure E-1, it is clear that the increased drops across A and B will be applied as a forward bias to the base-emitter junctions of A^1 and B^1 respectively, moving them from their off states towards their saturated regions. This reduced the drops across A^1 and B^1 which, from Figure E-1, reduces the forward bias applied to the base-emitter junctions of A and B respectively. Consequently, the base drives in transistors A and B are again decreased pushing them still farther out of saturation and increasing the drop across them. From Figure E-1 it is obvious that this increases the forward bias of A^1 and B^1 driving them farther into saturation which again reduces the bias applied to the base-emitter junctions of A and B.

Clearly, this process is self-supporting and it will continue until the drops across A^1 and B^1 becomes less than the voltage on the capacitor in the base circuits of A and B respectively. At this point, A and B are cut off, applying full forward bias to the base-emitter junction of A^1 and B^1 respectively. The circuit has now switched to the A^1B^1 conducting state and the voltage across and the current through the load have reversed in direction.

Since the circuit shown in Fig. E-1 is symmetric the maximum base currents in A^1 and B^1 respectively are given by:

$$I_{bi}(A^1) = \frac{V_{in} - V_s^{b1} - V_{ci}(A^1)}{R_{be}(A^1)} \qquad \text{(E-3)}$$

and

$$I_{bi}(B^1) = \frac{V_{in} - V_s^{a1} - V_{ci}(B^1)}{R_{be}(B^1)} \qquad \text{(E-4)}$$

As in the A B conduction state, these currents will decay exponentially as the capacitors in the base circuits of A^1 and B^1 begin to charge through their respective base-emitter resistances. As before, the base currents in A^1 and B^1 will decay to the value I_{b3} shown in Fig. E-2 and begin to move the transistors A^1 and B^1 out of their saturated states. Concurrently, the voltage that has been placed on the capacitors, C_1,

in the base circuits of A and B during the A B conduction state will be discharged by the resistors R_1, reducing the the reverse bias applied to the base-emitter junctions of A and B. The decreasing base drives in A^1 and B^1 will move them from the saturated state towards the "off" state and begin to apply a forward biasing potential to the base-emitter junctions of A and B respectively. When this applied forward bias exceeds the value of the decaying capacitor voltages in the base circuits of A and B, they will be moved toward their saturated regions, reducing the drop across them and hence reducing the forward bias on the A^1 and B^1 emitter-base junctions, further reducing the base drive in these transistors and moving them farther into their off condition. Again this process is clearly self-supporting and it follows that A^1 and B^1 will be cut off and the circuit returns to the A B conduction state from which the entire cycle is repeated.

Notice that a load (collector) current was chosen and held fixed for the above discussion. From Figures E-2, and E-3, we may now determine the effect of a change in load current on the oscillatory behavior of the circuit. Assume the load current is increased by holding V_{in} constant and decreasing R_L to give the value I_2 shown in Figure E-2. Then observe that an increase in base current to a value of I_{b5} is necessary to sustain the transistors in their saturated state. Since the maximum base current is dependent primarily on the input voltage and the respective base-emitter resistances, its magnitude will not be changed appreciably by the change in R_L. Therefore, it will be the same as shown in Figure E-3. From Figure E-3, we see that the decaying base drive in the transistors will reach the value I_{b5} at which switching will occur at a time t_1 that will be less than t_o, the time to reach I_{b4}. It is clear then, that an increase in load current has caused an increase in the frequency of the circuit oscillation.

In a similar fashion, an increase in the load resistance causing a decrease in load current to a value, I_3, will demand a lower base drive I_{b2} to maintain a saturated condition. The decaying base drive will reach the value I_{b2}at some time t_2 that is greater than t_o, at which point switching will occur. It is clear that the time between switching has been increased and hence the frequency of oscillation has been decreased.

We conclude that the frequency of the circuit oscillation is dependent upon the value of base current that is necessary to sustain each of the transistors in its conducting state. The functional form of this dependence is given by:

$$f = \frac{1}{2}\left[\frac{R_1 R_{be} C_1}{R_1 + R_{be}}\right]^{-\frac{1}{2}} \quad \frac{1}{\log \frac{I_{bi}}{I_{bo}}}$$

$$R_1 >> R_{bi} \qquad \text{(E-5)}$$

where I_{bi} and R_{be} are general representations of the quantities defined previously, and I_{bo} is the value of base current below which the transistor switches from the conducting state to the non-conducting state.

From Figure E-2,we see that the value of I_{bo} is a function of the collector current of the transistor. In general, this relation must be obtained from graphs of the transistor characteristics.

The choice of transistors is the most important design consideration, To achieve a smooth, balanced operation, a matched set of PNP's should be used for transistors A and A^1 and a matched set of NPN's for transistors B and B^1. In addition, these sets should be complementary. The frequency relation given above assumes this symmetry.

Conclusions:

This circuit presents several advantages over other available oscillator designs; it exhibits high efficiency at relatively high power levels, and it is simple and compact. In addition, the circuit's reliability should be high since it contains only simple resistor-capacitor combinations and solid state devices.

The following table lists a typical oscillator design:

Transistors:

PNP	2N-1042
NPN	2N-1702

V_{in}	20V
R_l	11.5 to 25 ohms.
Power out	30 watts
Max. Eff.	80% $\pm$ 3%
Frequency Range	7.0 - 30.0 kilocycles
R_l	1000 ohms
C_l	0.01 micro-farads

Appendix F

PHYSICAL DESCRIPTION OF TEST TRANSFORMERS

Two air-core transformers (hereinafter referred to as T1 and T2) were designed, built, and tested. The designs possessed the following characteristics.

T1: Toroidal radius = R = 1.25 inches

Cross sectional radius = a = 0.25 inches.

Number of layers of Primary turns = 2

(1) turns layer 1 = 537

(2) turns layer 2 = 507

Number of layers of Secondary turns = 2

(1) turns layer 1 = 700

(2) turns layer 2 = 690

Wire size of Primary = #28 Awg, with 1 mil thick insulation.

Wire size secondary = #30 Awg. with 1 mil thick insulation.

Inter-layer insulation thickness = 3.5 mils.

Permittivity of all insulation = $2\varepsilon_0$

Load Resistance = 1.0 K and 30.4 K.

T2: Toroidal radius = 1.25 inches

Cross sectional radius = a = 0.25 inches

Number of layers of primary turns = 2

(1) turns of layer 1 = 440

(2) turns of layer 2 = 431

Wire size for both primary and secondary is #28 awg, magnet wire with 1 mil insulation thickness

Interlayer insulation thickness = 3.5 mils.

Permittivity of all insulation = $2\varepsilon_o$.

Load Resistance: (a) 1.0k ohms and (b) 30.4 k ohms.

Number of layers of secondary windings = 8

(1) turns of layer 1 = 423
(2) turns of layer 2 = 415
(3) turns of layer 3 = 406
(4) turns of layer 4 = 398
(5) turns of layer 5 = 389
(6) turns of layer 6 = 381
(7) turns of layer 7 = 372
(6) turns of layer 8 = 364

The analysis of these models was based on the assumption that the individual turns in a given layer of the winding are in contact along the inner circumference of the toroid and diverge toward the outer circumference in a uniform manner. The fabrication of the transformers adhered to this principle within tolerance limits imposed by precision of the winding procedure.